CERN-PPE/91-195
22 October 1991

EUROPEAN ORGANIZATION FOR NUCLEAR RESEARCH

The Performance of a Lead/Scintillating-Fiber Calorimeter at LHC/SSC Compatible Gate Widths

D. Acosta[1)], P. Avellino[2,3)], S. Buontempo[4)], L. Calôba[5)], R. DeSalvo[6a)], A. Ereditato[4)], R. Ferrari[7)], G. Fumagalli[7)], G. Goggi[6,7)], W. Hao[8)]†, A. Henriques[2,6)], L. Linssen[6a)], M. Livan[9)], A. Maio[2)], M.R. Mondardini[10)], B. Ong[1)], H.P. Paar[1)], F. Pastore[7)], E. Pennacchio[7)], L. Poggioli[6,11)], G. Polesello[6,7)], F. Riccardi[4)], A. Rimoldi[7)], C.V. Scheel[6a,12)], J.M. Seixas[5,6)], A. Simon[13)], C. Silva[2,3)], M. Sivertz[1)], P. Sonderegger[6)], M.N. Souza[5)], Z.D. Thomé[5)], V. Vercesi[7)], Y. Wang[8)]†, R. Wigmans[6,12)] and C. Xu[8)]†

1) *University of California, San Diego, USA*
2) *LIP, Lisbon, Portugal*
3) *Universidade do Porto, Porto, Portugal*
4) *Università di Napoli and INFN Sez. Napoli, Italy*
5) *COPPE/EE/UFRJ, Rio de Janeiro, Brazil*
6) *CERN, Geneva, Switzerland*
6a) *CERN/LAA project, Geneva, Switzerland*
7) *Università di Pavia and INFN Sez. Pavia, Italy*
8) *Worldlab, Lausanne, Switzerland*
9) *Università di Cagliari and INFN Sez. Cagliari, Italy*
10) *Cornell University, Ithaca, USA*
11) *LPNHE, Université Paris VI&VII, Paris, France*
12) *NIKHEF-H, Amsterdam, the Netherlands*
13) *Universität Heidelberg, Heidelberg, Germany*

† On leave of absence from IHEP Beijing, China

Abstract

We report on an experimental study of the performance of a lead/scintillating-fiber calorimeter intended for the detection of leptons, hadrons, gammas and missing energy. In particular, the effects of reducing the charge collection time down to values that are relevant for experiments at the future proton-proton colliders LHC and SSC are investigated. The total calorimeter signal, the energy resolution, the e/π signal ratio, the signal linearity, the hadronic shower profile and the electron/pion separation capability of the detector are measured as a function of the charge collection time, ranging from 5 to 358 ns. The performance is practically unaffected down to ~ 40 ns, even when unrealistically long signal cables are used and no signal shaping is applied. For shorter gates, we observe incomplete charge collection, a gradually deteriorating energy resolution, an increase in the e/π signal ratio and in the hadronic signal alinearity, a narrowing of the hadronic shower profile and a degradation of the electron/pion separation. However, even for gates as short as the LHC/SSC bunch-bunch spacing (~ 15 ns), these effects are not unacceptably large. The experiments were performed in the framework of the LAA project at CERN.

This paper is dedicated to the memory of Vittorio Vanzanella, in whom we lost an outstanding engineer and a good friend

(Submitted to Nuclear Instruments and Methods in Physics Research)

1. *INTRODUCTION*

The detectors to be installed in the future multi-TeV pp colliders LHC and SSC will face unprecedented event rates. The cross sections for the physics processes of interest are at best at the 1 pb level and, in order to collect a sufficient rate of interesting events, luminosities in the $10^{33-34}\mathrm{cm}^{-2}\mathrm{s}^{-1}$ range are envisaged[1] . For a total pp cross section of 100 mb, this translates into primary event rates of 10^{8-9} Hz. The bunch spacing in these machines is $\sim$ 15 ns, so that multiple interactions in the same bunch crossing will frequently occur.

Such high event rates will cause a multitude of problems for the detectors and the associated data acquisition systems. These will have to match the speed of the incoming information and, therefore, the signal speed of the detectors is an important issue. Two aspects should be distinguished in this respect:

1) The signal *timing*.

2) The signal *duration*.

The first aspect determines the accuracy with which the information coming from a certain detector can be assigned to a specific bunch crossing. The difficulties concerning this point are not only determined by the intrinsic detector properties, but also by the cabling, which has to account for the time it takes particles to reach different detector elements and for the time it takes signals to reach the point where the assignment is made. It has been shown[2] that thanks to the possibilities offered by pulse shaping techniques even intrinsically very slow detectors are not limited in this respect. The second aspect, the signal duration, is the subject of this paper. We mention two items that are directly affected by it:

a) Each event, or rather the combined events occurring in the same bunch crossing, will have to be examined individually in order to see whether the event information justifies a more careful study. In principle, only 15 ns are available, although the period needed for actually making the first-level trigger decisions may be stretched using parallel trigger processors and pipeline techniques. The question arises how representative the information collected in this short time really is for the event. It may be expected that this will be less of a problem if a good fraction of the charge characterizing the event is collected in this period.

b) Because of multiple interactions per bunch crossing, pile-up of unrelated events will inevitably occur. However, the problems caused by this phenomenon will drastically increase if the charge collection time of each event spans many bunch crossings.

While event pile-up will be a problem for all LHC/SSC detectors, the first item is specific for detectors participating in the first-level trigger decisions. Such decisions are

expected to be mainly based on the data provided by the calorimeters and, therefore, the signal speed of the calorimeters is particularly important.

The Spaghetti Calorimeter was developed, in the framework of the LAA project at CERN, as a dedicated calorimeter for LHC/SSC experiments. It is an (almost) compensating lead/scintillating-fiber calorimeter with monolythic towers, i.e. without longitudinal segmentation into an electromagnetic (e.m.) and an hadronic section. Several of its remarkable properties are described elsewhere.[3–9] These properties include a very high signal speed. Detectors based on scintillation light are among the fastest ones available for particle physics experiments. Calorimeters using scintillating fibers as the active medium have the additional advantage that no external wavelength shifters are needed in order to bring the light to a place where it can be detected, as for example in plate calorimeters. Such wavelength shifters tend to slow down the charge collection.[10] In earlier studies we exploited the high signal speed of the fiber calorimeter successfully for particle identification, using the fact that the signals from hadronic showers are somewhat slower than e.m. ones[3,5] . By measuring the pulse widths at 20% of the amplitude, e/π separation at the 10^{-3} level was achieved[5] .

All our earlier studies were, for practical reasons, done with a gate width for the analog-to-digital converter (ADC) of 400 ns, largely sufficient to collect all the produced charge. In this paper, we investigate the effects on the calorimeter performance of reducing this gate width, to values relevant for operation at LHC/SSC. This study has to be regarded as exploratory. We did not try in any way to improve the short-gate performance of the calorimeter, which from experience with other types of calorimeters is known to be possible by properly shaping the signals[2] . As will be shown in the following sections, the obtained results are quite strongly affected by the fact that very long signal cables of rather poor quality were used for the measurements. If and when possible, we estimated the effects of these cables on the experimental results. For the rest, we present the results as obtained in this particular setup and leave the optimization of the short-gate performance of this intrinsically very fast datector to future, dedicated studies. In section 2, the detectors, the experimental setup and the trigger and data acquisition system are described. Section 3 deals with the experimental data and with the methods that were used to eliminate the instrumental effects that complicated the study of the short-gate performance. Experimental results on the effects of the gate width on the collected charge, the energy resolution, the e/π signal ratio, the signal linearity, the measured shower profiles and the electron/pion separation capability of the calorimeter are presented in sect. 4. A summary and conclusions are given in section 5.

2. EXPERIMENTAL SETUP

2.1 The detector

The measurements were performed with a calorimeter consisting of longitudinally unsegmented towers. Each tower contains 1141 plastic scintillating fibers* with a diameter of 1 mm and a length of 2.20 m. These fibers form the active part of the sampling calorimeters. They are embedded in a lead matrix in such a way that each fiber is equidistant to its 6 neighbors (fig. 1a). The fiber spacing is 2.22 mm (center to center), such as to achieve a volume ratio lead:fiber of about 4:1, needed in order to make the calorimeter (approximately) compensating.[11,12]

The fibers were grouped to form towers. Each tower has an hexagonal cross section (86 mm apex to apex). The depth of the lead structure is 200 cm. The fibers sticking out at one end of the tower were bunched together in an hexagonal structure, machined and polished and coupled through an hexagonal light guide (79 mm long, 42 mm apex to apex) to a photomultiplier (PM)** . The other ends of the fibers were polished and made reflective by aluminium sputtering, such as to make the response more uniform as a function of the position along the fiber. More detailed information about the structure of the calorimeters is given in ref. 4.

The calorimeter contains 155 towers. A central tower is surrounded by 7 concentric hexagonal rings (see fig. 1b); with the outer ring incomplete, the detector has roughly a cylindrical shape with a diameter of 1 meter. In the experiments described in this paper, the calorimeter was installed as intended in experiments for which it was developed, namely with the fibers running in (almost) the same direction as the beam particles and the readout located at the back end of the detector. Expressed in units of the nuclear interaction length λ_I[13] , its dimensions amounted in this way to 9.5 λ_I in depth and 4.8 λ_I across. A smaller (20-tower) prototype of the same structure was used in conjunction with it. Installed behind the main calorimeter, it served as a leakage calorimeter[9] . For the analysis described in this paper, the information from this leakage calorimeter served mainly to identify and remove beam muons contaminating the event samples.

The PM signals were handled as follows (see fig. 2). The anode signal from each individual tower was split into 2 equal parts by means of a passive splitter inside the base. One part went to the counting room where it was further fed into an active splitter (called OLIFAN), one output of which was buffered and sent into a 12-bit charge ADC,† the other output was amplified by a factor $\sim$ 10 before being fed into an ADC. The

* SCSF-38, produced by Kyowa Gas, now Kuraray Co. Ltd, Tokyo, Japan

** Philips XP 2282B, 8-stage

† Lecroy system 2280, with 2282E modules

other half of the anode signal went into a linear adder[‡] , where it was combined with tower signals from the same hexagonal ring. The resulting ring sum signals were treated in the same way as the signals that were directly sent to the counting room. The signals of the leakage calorimeter were only split at the ADC level, but not inside the PM base.

The calorimeter was calibrated with 40 GeV electrons at an ADC gate width of 400 ns. About 1500 electrons were sent into the central region of each of the 155 individual towers. The gain in the PM tubes was set to deliver ~ 4 pC/GeV in the central detector region, gradually going up to ~ 20 pC/GeV in the outer rings of the calorimeter, for the unamplified channels. The ADC gain was 4 counts/pC. This procedure was chosen to circumvent the insufficient dynamic range of our PM/ADC system and to be sensitive to small energy deposits far away from the shower axis.

2.2 The beam line

The measurements were performed in the H2 beam line of the SPS at CERN. The calorimeter was mounted on a platform that could move horizontally and vertically with respect to the beam line, with a precision of about 1 mm. Moreover, the detector could be rotated around its vertical axis, so that the particles could be sent into the detector at a chosen angle θ_z (usually a few degrees) with respect to the fiber axis. The precision of the angular movement was better than 0.1 mr, although the precise value of θ_z was only known to about 10 mr[9] . About 12 cm upstream of the calorimeter, a preshower detector was mounted. This preshower detector (PSD) consisted of an absorber sheet (1.14 X_0 tungsten + 0.53 X_0 lead), followed by a scintillation counter (S6). The signal in this scintillator provided a clean (at energies of 40 GeV and higher about a factor 10) separation between electron and pion events[5] . Further upstream of the calorimeters, a trigger counter telescope was installed. It consisted of 5 scintillation counters (S1 - S5). The beam particles were tracked by two drift chambers with x,y readout (BC1, BC2). The layout is shown in fig. 3.

For the tests described in this paper, beams of 80 GeV electrons and negative pions of 40, 80 and 150 GeV were sent into the detector at a small angle θ_z. The beam particle rates were $10^2 - 10^3$ events per spill. The spills lasted for 2.6 s and were repeated every 14 s.

At these high energies ($\geq$ 40 GeV) the beams were very clean, the contamination of electrons (pions) in the pion (electron) beam being below the 1% level. The few contaminating particles could be efficiently removed with the help of the PSD data. The pion beams also contained some small ($<$ 10%) fraction of muons. These muons

‡ Lecroy 628

were removed from the event samples with the help of the leakage calorimeter, in which they produced a very characteristic signal[9] .

Off-line event selection required a single track, by cutting on the pulse height of the scintillation counters S1,2,3 between 0.5 and 1.7 times the minimum ionizing particle (mip) value. The x and y coordinates measured in the two beam chambers had to agree within 1 cm. Beam halo particles were removed by cuts on x and y in the beam chambers.

2.3 Triggering and data acquisition

The trigger was provided by a coincidence of signals in the counters S1, S2, S3, S4 and S5. This coincidence signal opened the ADC gate. The lengths of the various cables were such that this signal arrived in the counting room about 40 ns before the signals from the calorimeter towers. The calorimeter signals were transported to the counting room by means of standard coaxial cables* with a characteristic impedance of 50Ω , with a length of $\sim$ 100 m (signal transport time $\sim$ 500 ns). For this study, we had to make sure that all the signals from the different calorimeter towers arrived in the ADC's at the same point in time, which was initially not the case, for example because of small differences in the cable lengths and in the transit times of the PM's. The time differences between the trigger signal and the signals that were fed into the various ADC's were equalized by delaying the latter ones by adequate amounts, typically a few nanoseconds.

Electrons of 20 GeV were sent into the towers to be timed. Because of the time involved with this procedure, we did not equalize the arrival times for all 155 towers. Only the central tower and the 18 towers from the two innermost rings (see fig. 1b) were treated individually. For the other rings, one tower was chosen for each ring and the arrival times of the ring sum signals (see fig. 2) were equalized. This meant that the signals from towers in the outer parts of the detector could not be studied individually (since their cables were not properly timed), but only as part of an (hexagonal) ring. In principle, differences in the timing properties between towers in the same ring could in this scheme still be caused by the PM's, which operated at different voltages, but the jitter arising from this effect was estimated to be smaller than 1 ns. It turned out that also the circuits that split and amplify the PM signals and send them to the high-gain and low-gain ADC's had a noticeable effect on the timing, in the sense that both signals did not arrive at the same time at their respective ADC's. We decided to time in only one of these signals. For the central tower (the one hit by the beam) the unamplified channel was chosen for this purpose, for all other towers the amplified channels were taken.

* Type RG-58C/U

The time equalization method, which was carried out with an oscilloscope, was accurate to within ~ 0.5 ns. After its completion, at least one of the four signals from each calorimeter tower (see fig. 2) arrived at the ADC input 42 ± 1 ns after the trigger signal. This value, determined by the relative lenghts of the signal cables from the trigger counters and from the calorimeter towers, and chosen unnecessarily long for these measurements, should in a real LHC/SSC experiment of course not exceed a few ns. When, in the following, we quote a value for the gate width, we always mean the time during which the charge of the calorimeter signals was collected. Strictly speaking, this is the real ADC gate width minus 42 ns.

Since the ADC's were operated at gate widths smaller than the range for which the linearity was specified (100 ns), we checked the linearity of the response for the gate widths used in this study. The alinearity turned out to be negligible compared to other experimental uncertainties encountered in this analysis. For each gate width, the pedestal values of the ADC's were determined in separate runs. Sparse data readout was enabled: signals smaller than 4 counts above the pedestal value were not recorded. This corresponds to a cutoff of 5 MeV energy deposits in the amplified channels of the outer detector rings (see sect. 2.1).

3. EXPERIMENTAL DATA AND METHODS

3.1 Experimental data

The results described in the following sections were obtained by analyzing the following sets of data:

- Pions and electrons of 80 GeV entering the calorimeter at an angle $\theta_z = 3^0$ to the fiber axis. Data were taken for the following gate widths: 2, 5, 10, 15, 20, 25, 30, 39, 58, 108, 154, 251 and 358 ns. Typically, ~ 3000 events were accumulated per run.
- Pions of 40, 80 and 150 GeV entering the calorimeter at $\theta_z = 3^0$, for a gate width of 16 ns. Also here, ~ 3000 events were recorded at each energy.

Pure samples of electron and pion events were obtained by using data from the PSD and the leakage calorimeter. Muons were efficiently removed from the event samples by requiring that less than 125 MeV be deposited in the leakage calorimeter[9] . The signal in the PSD was required to be less than 2 mip for pions and larger than this value for electrons.

Some of the results obtained from this analysis could be checked independently with data on the explicit time structure of the calorimeter signals, obtained with the 20-tower prototype (sect. 2.1) at an earlier stage[5] . The signals from 80 GeV electron and pion

showers were recorded with a fast digitizing oscilloscope* , in time slices of 1 ns, for this purpose. The particles were sent into the central cell of the calorimeter and the measurements concerned the linear sum of the signals in this central cell and its six neighbors.

3.2 Unfolding the cable effects

When a fast electronic signal is transported through a cable, the signal shape is affected. Both the rise time and the decay characteristics are changed[14] . The long signal cables and their relatively poor quality had a considerable effect on the calorimeter signals. In a realistic application of this detector in an LHC/SSC experiment, where signal digitization will certainly be done at the frontend, such effects would be absent or at least greatly reduced. In order to obtain a realistic impression of the detector performance under such circumstances, we determined the effects of the cables on the calorimeter signals and unfolded these effects from the experimental results. The effects of the cables were determined by measuring and analyzing the cable response $r(t)$ to a fast step function (rise time less than 1 ns, see fig. 4a). The signal cable normally connected to the output of one of the PM tubes was connected to the output of a fast pulse generator** for this purpose. The signal was measured at the counting room end of the cable (fig. 4b). The effects of the cable are considerable. The rise time, defined as the time Δt it takes to go from $r(t) = 10\%$ to $r(t + \Delta t) = 90\%$ of the total integrated charge, amounts to $\sim$ 65 ns. In addition, the time it takes to go from 90% to 99% is a multiple of this number, so that the cable introduces very long tails to the signals. These effects were unfolded using methods from circuit theory, as described in detail in Appendix A. After unfolding the cable effects from the measured step response, the original step function was reasonably well reproduced (see fig. 4c).

When, in the following, we show experimental results for which the cable effects have been unfolded, the actually measured data are shown as well, so that the effects of the cables on the measured calorimeter properties can be appreciated.

3.3 Data handling

In sect. 2.3 we described how the arrival times of the signals from the different calorimeter towers were equalized. From each tower, at least one signal arrived at the ADC input within one nanosecond of the signals from the other towers. This turned out to be crucial for the results from measurements in which the charge collection time was so short that a significant fraction of the signal arrived at the ADC after the gate

* Hewlett Packard 54111D, 1 GSample/s, 500 MHz bandwidth

** Tektronix 284

was closed. This is illustrated in figs. 5 and 6, which show results of measurements on 80 GeV pions entering the calorimeter in the central tower at $\theta_z = 3^0$.

Figure 5 shows the signals measured in the fourth hexagonal ring, which consists of 24 towers. The (amplified) ring sum signals, which are transported to the counting room through one, properly timed cable are displayed versus the (amplified) signals obtained by adding the signals from the 24 individual towers, which are transported to the counting room through 24 individual signal cables and which were not properly timed. For a long ADC gate (fig. 5a) there is an excellent correlation between these two signals, to be called the hardware sum (HS) and the software sum (SS) in the following. The data points in the scatter plot cluster on a line at 45^0 to the origin. When the gate is shortened to the point where a significant fraction of the charge is not collected, the SS signals become systematically smaller than the HS ones. Due to differences in the timing of the individual signals, the SS signal is broadened and a larger fraction of it arrives beyond the gate (fig. 5b).

A similar phenomenon is observed in fig. 6, where the signals in the amplified and non-amplified channels are compared. For a long gate, there is again an excellent correlation between these two signals (fig. 6a,c). For a short gate, the signal that was timed is systematically larger than the other one.

It turned out that the effects shown in fig. 6 are not entirely due to the timing of the signals. Detailed measurements with generated pulses revealed that the OLIFAN active splitters generated some noise, which affected the charge collection characteristics of the ADC's. This noise was similar for the amplified and unamplified outputs, and the charge collection was significantly slower for small signals from the latter. This produces effects similar to the ones shown in figs. 5 and 6. More detailed information about these effects is given in ref. 15.

Throughout the data analysis described in the following chapter, we only used the signals whose arrival times at the ADC input were equalized, i.e. for the central tower the unamplified channel, for the first and second hexagonal rings the amplified SS signals and for the other rings the amplified HS signals.

4. EXPERIMENTAL RESULTS

In this section, we describe the results of the analysis of the calorimeter performance as a function of the gate width. Several of the calorimeter's properties discussed in this section were investigated in detail before[5,8], for a gate width of 358 ns. In these cases, the emphasis in the presentation of the results will be on the *relative* effects induced by the short gate. For the absolute values of the measured quantities, the reader is referred to the original publications.

4.1 The calorimeter signals

In this subsection, we discuss the calorimeter signal, i.e. the integrated charge, as a function of the time during which the signal is integrated. The results are normalized to the ones obtained for a gate of 358 ns, which turned out to be sufficiently long to collect all the charge. This was checked with a measurement over 658 ns. The signals for a 658 ns gate were not significantly larger than at 358 ns.

The results of the measurements are shown in fig. 7a, where the signal is given as a function of the charge collection time, for 80 GeV electrons and pions entering the central calorimeter tower at an angle $\theta_z = 3^0$. From fig. 4b it is clear that these results are considerably affected by the signal cables. After unfolding these effects, in the way described in Appendix A, the results shown in fig. 7b were obtained. It turns out that 90% of the charge is collected in 37 ns for electrons and in 47 ns for pions. In 16 ns, the LHC/SSC bunch spacing, typically 75% of the charge generated by electromagnetic showers is collected and 67% of the hadronic charge. The numerical results are summarized in Table 1.

The difference between the charge collection times for e.m. and hadronic showers is small but very significant. It is due to two effects[3] :

1) The production of scintillation light occurs for hadronic showers on average deeper inside the calorimeter than for e.m. ones. Part of the signal is due to light that is reflected at the mirror on the upstream front face of the fibers. This leads to a significant broadening of the hadronic shower signals, and frequently even to a double-hump signal structure[5] .

2) A considerable fraction of the hadronic signal is caused by soft neutrons originating from nuclear evaporation processes[11] . These neutrons lose their kinetic energy through elastic collisions with hydrogen nuclei in the plastic scintillator, a process with a time constant of ~ 10 ns[5] .

In the earlier studies mentioned we exploited these differences for e/π separation. The charge collection curves from fig. 7b may be compared to similar results obtained in a completely different way. Calorimeter signals from 80 GeV electrons and pions were studied with a fast digitizing oscilloscope. The signals from the central tower and the six towers of the innermost hexagonal ring were linearly added together and sent as one signal to the oscilloscope for this purpose. The signals were transported to the oscilloscope through a very fast cable* , with a length of 30 m. The rise time for a step function sent through this cable amounted to only 6 ns, as opposed to 65 ns for the standard signal cables. The effects of this cable were unfolded with the same procedure as before (Appendix A). The oscilloscope yields sampled information on the

* Type C-50-6-1

signal structure, in time slices of 1 ns. By integration one may obtain charge collection curves similar to the ones in fig. 7. In this exercise, it is very important to know the base line of the pulses, i.e. the 100% level of the collected charge. This level was determined from the average scope reading in the 50 ns preceding the start of the pulse.

Figure 8 shows results of these measurements, for signals from the central region of the calorimeter. Also in this case, where the contribution of neutrons, which deposit their energy mainly in the more outward parts of the detector, is suppressed, a clear difference in the charge collection characteristics between signals from e.m. and hadronic showers is observed. Ninety percent of the charge is collected in 31 ns for electrons and in 37 ns for pions. The fact that the charge collection time appears to be a bit shorter than for the ADC measurements may be due to the fact that the oscilloscope's data acquisition chain had a considerably larger bandwidth.

Table 2 summarizes the results on the charge collection time measured for different types of signals before and after unfolding the effects of the signal cables.

4.2 The energy resolution

The energy resolutions for electron and pion detection with this detector were measured before, for a 358 ns gate. We found $\sigma/E = 12.9\%/\sqrt{E} + 1.2\%$ for electrons and $30.6\%/\sqrt{E} + 1.0\%$ for pions[8] . The latter result was obtained after correcting for the effects of light attenuation in the fibers, which increase the energy independent term.

The energy resolution was studied as a function of the charge collection time for 80 GeV electrons and pions. The results are given in Table 3, for the various gate widths used in this study. The energy resolutions are normalized to the ones obtained for a 358 ns gate. Figure 9 shows the energy resolution for 80 GeV electrons. It turned out that for very short gates, when a significant fraction of the signal arrives beyond the gate, deviations from a Gaussian response curve occur (fig. 10). Therefore, the σ obtained from a Gaussian fit differed from σ_{RMS}. This effect becomes insignificant for gates longer than 40 ns, which is sufficiently long to collect practically all the charge. Figure 9 shows that the resolution remains practically constant (less than 10% deterioration) down to gate widths of $\sim$ 25 ns. For shorter gates, the resolution gets rapidly worse.

Similar phenomena were observed for pions (fig. 11), albeit that the deterioration of the resolution starts at gates that are slightly longer than for electrons. This should be expected since it takes more time to collect a sufficient fraction of the charge for pions.

Some dedicated measurements were done for a gate width of 16 ns, an interval close to the LHC/SSC bunch spacing. Pions were measured at three different energies: 40, 80 and 150 GeV. The energy resolution is shown as a function of the energy in fig. 12. For comparison, the resolutions for 358 ns are given as well. The latter, obtained from

the analysis of the ring sum signals, can be described as $\sigma/E = 29.5\%/\sqrt{E} + 2.2\%$ and are not significantly different from the results derived previously from analysis of all the individual cell signals ($\sigma/E = 27.7\%/\sqrt{E} + 2.5\%$)[8] . The resolution for a gate width of 16 ns is worse by about a factor of 2.

The mentioned results concern uncorrected data. Since we are interested in the relative effects of a reduction of the charge collection time, we did not apply for each separate gate width the corrections usually made to evaluate the energy resolution, such as the effects of energy loss in the PSD (e.m. showers) and light attenuation in the fibers (hadron showers). Since such corrections are expected to be in first approximation independent of the gate width, we used the experimental data at face value for this analysis. Also, the results shown in this subsection were not corrected for the cable effects, since this is not possible for this type of data. However, since the charge collection can be considerably speeded up with faster or shorter signal cables (figs. 7,8) and since the deterioration of the energy resolution is due to incomplete charge collection, one may expect that the energy resolution results shown in figs. 9-10 would further improve if better and shorter signal cables were used for these measurements.

4.3 The e/π signal ratio

The e/π signal ratio of this detector was measured before to be 1.028 ± 0.001 (stat.) at 80 GeV, for a 358 ns gate[8] . For similar measurements analyzed in this paper we found a value of 1.013 ± 0.001. These values concern the e/π signal ratio as measured, i.e. before applying a number of (small) corrections accounting for systematic effects.[8] The small difference is probably due to the fact that very small contributions to the signals, which are cut off by the requirement that at least 4 ADC counts above pedestal should be recorded in the calorimeter channels (see sect. 2.1), were less suppressed in the present analysis: the calorimeter channels corresponded to complete hexagonal rings, as opposed to individual towers[8] . This mainly affected the hadronic signals, which increased a little bit, thus reducing the e/π signal ratio somewhat.

In Table 4, the e/π signal ratios are listed for the various gate widths used in this study. Both the results obtained before and after unfolding the cable effects are given. Figure 13 shows how the e/π signal ratio changes as a function of the charge collection time. As for the energy resolutions, the relative effect of the gate is shown and, therefore, the e/π signal ratios are normalized to the value for a 358 ns gate. When the gate is shortened, the e/π signal ratio is observed to increase. This is a consequence of the different signal shapes. Since it takes more time to collect the charge from an hadronic shower than from an e.m. one, incomplete charge collection resulting from a short gate will cut a larger fraction of the hadronic signals. However, this effect is marginal down to gates that are much shorter than 358 ns. At 25 ns, the increase in the e/π signal ratio is only 8.8% (6.7%) for uncorrected (cable unfolded) signals. For shorter gates,

the ratio rapidly increases. The stretching effect of the cables on the calorimeter signals turns out to have little influence on the e/π signal ratio.

4.4 The hadronic signal linearity

For very short gates, the calorimeter becomes strongly undercompensating. Apart from the deterioration in the hadronic energy resolution (see fig. 11), this also causes signal nonlinearity for hadronic shower detection. The reason is the following. The π^0-component of the hadronic showers is produced closer to the calorimeter front face and develops faster than the nonelectromagnetic shower component. When the charge collection is truncated, a larger fraction of the charge associated with the π^0-component will therefore be collected than for the nonelectromagnetic shower component. And since the average fraction of the shower energy that goes into π^0 production increases (roughly logarithmically) with the energy, the total signal per GeV increases as well (antilinearity). This effect was clearly observed (fig. 14). For a 16 ns gate it amounts to about 25% over an order of magnitude in hadronic energy. This is comparable to the antilinearity observed in typical undercompensating iron calorimeters[16] .

4.5 The hadronic shower profile

The shortening of the charge collection time has an interesting effect on the hadronic shower profiles. Recalling the arguments why hadronic signals are slower than e.m. ones (sect. 4.1), one may expect the charge from the shower tails to arrive on average somewhat later than the charge from the shower core, because

a) The light producing the charge in the shower tails is generated deep inside the calorimeter and therefore its reflected component is delayed with respect to the reflected component of the light generated in the shower core.

b) The light producing the charge in (both the longitudinal and the lateral) shower tails is predominantly caused by elastic neutron scattering and is therefore delayed with respect to the prompt light generated by the e.m. component dominating the shower core.

As a consequence, truncation of the charge collection by means of a short gate will cut a larger fraction of the signal from the shower's tails than from its core and the shower appears to be narrower, both longitudinally and laterally. Since the calorimeter is longitudinally unsegmented, we only studied the lateral effect, which was clearly observed.

Lateral shower profiles for 80 GeV pions at a long (358 ns) and a short (20 ns) gate are shown in fig. 15. These profiles represent the energy density as a function of the distance from the shower axis. In practice, we used the summed signals from the hexagonal rings for this purpose and divided these by the number of calorimeter cells

in the ring. The profiles exhibit a pronounced core and an exponential tail. Reduction of the gate width reduces the tail more than the core.

In order to quantify this effect, the profiles were fitted to an expression of the following type:

$$f(r) \;=\; B_1 \exp(-r/\lambda_1) \;+\; B_2 \exp(-r^2/\lambda_2^2) \tag{1}$$

which turned out to give an accurate description of much more detailed measurement results of such profiles[8,17] . From these fits, we determined the ratio of the contributions of the exponential and Gaussian components, E/G, to the signal:

$$E/G \;=\; \frac{\int_0^\infty B_1 \exp(-r/\lambda_1)\; dr}{\int_0^\infty B_2 \exp(-r^2/\lambda_2^2)\; dr} \tag{2}$$

The values of the parameters B_1, B_2, λ_1 and λ_2 and the values of the ratio E/G are listed in Table 5, for the various gate widths used in this study. In this analysis, the effects of the signal cables could be unfolded. The charge collection curve for each of the individual ring sum signals was corrected in the way described in Appendix A. Both the results obtained before and after unfolding the cable effects are given. The table shows that the values of λ_1 and λ_2, defining the shape of the two components of the shower profile, are insensitive to the charge collection time and the cable effects. On the other hand, the relative contributions of these two components are sensitive, in particular to the gate width. Figure 16 shows the ratio E/G as a function of the charge collection time, both for the results obtained from fits to the uncorrected and the corrected profiles. As expected, this ratio decreases when the charge collection is truncated.

This shrinking of the hadronic shower profiles might have potential advantages, such as improved position resolution and spatial particle-particle separation capability[6] . It also means that the e/π signal ratio is less strongly dependent on the cluster size, i.e. the lateral area over which the calorimeter signals are integrated. This is illustrated in figs. 17 and 18. In fig. 17, the e/π signal ratio is shown as a function of the cluster size, for various gate widths. When the area is reduced, the relative increase of the e/π signal ratio is clearly smaller for short gates (fig. 18). However, the absolute e/π signal ratios obviously increase for any cluster size when the charge collection time is reduced.

4.6 The electron/pion separability

One potential disadvantage of the fact that the hadronic shower profiles get narrower when the charge collection is truncated concerns the electron identification capability of the detector. Because of its fine transverse granularity, exploiting the differences in the lateral shower profiles is a powerful tool for this purpose. In previous studies[5,6] we demonstrated that electrons and pions can be efficiently separated with a variety

of quantities measuring the effective lateral width of the shower. Typically, hadron rejection factors ranging from 300 to 1000 were obtained, for an electron efficiency of $\sim 99\%$.

In this analysis, we define the effective shower radius simply as

$$R = \frac{\sum_i r_i E_i}{\sum_i E_i} \tag{3}$$

where E_i is the energy deposited in an individual tower i and r_i is the distance between the center of the tower i and the center of gravity of the shower. Only 37 towers, the central one plus the first three hexagonal rings were used to calculate R. Adding more rings did not significantly change the e/π separation. For energy deposited in the third ring, where only one signal was available, a value $r_i = 206$ mm was used, which corresponds to the average distance between the detector center and the area covered by this ring. The average radius for electron showers was found to be 25 mm when determined in this way, whereas for pions it ranged from 58 mm at 358 ns to 52 mm at 10 ns. Because of the low statistics and the good e/π separation, only a small number (typically 10) of pion events passed the R cuts defined to obtain an electron efficiency of 99%. Therefore, the pion rejection factors obtained from this analysis have large statistical uncertainties. The pion rejection factor is shown as a function of the charge collection time in fig. 19. Due to the large error bars, the effects are not very significant. Nevertheless, the pion rejection factor for short gates seems to be systematically smaller (by a factor of 2-4) than for long gates, in agreement with expectations.

Another technique used for electron/pion separation exploits the differences in the signal shapes of the showers[5] . By measuring the width of the pulses at 20% of the amplitude (FWFM), a pion rejection factor of 800 was achieved at an electron efficiency of 99%. The characteristic FWFM of an electron shower signal amounts to ~ 13 ns and, therefore, this method breaks down for charge collection times shorter than ~ 20 ns. Figure 20 shows how the pion rejection factor changes as a function of the gate width, for a constant electron efficiency of 98%. These results were obtained from the analysis of shower signals measured with the oscilloscope, which sampled them in time slices of 1 ns. The effect of a reduction of the charge collection time was therefore studied with one and the same sample of events for each gate width and no error bars could be assigned to the experimental points. Only ten pion signals passed the electron criteria for gates longer than 20 ns in this analysis. It has been shown before[5] that if the effects of all components in the data acquisition chain are filtered out, the "intrinsic" FWFM of an e.m. shower signal amounts to ~ 8 ns. Electron-pion separation could, therefore, continue to be achieved down to ~ 15 ns with this technique if such filtered pulses were available (fig. 20). Also, the actual pion rejection factors could be increased by about 30% using such filters[5] .

5. SUMMARY AND CONCLUSIONS

We have studied the performance of a lead/scintillating-fiber calorimeter as a function of the time during which the charge of the signals is collected. This study was inspired by the possible application of such a detector in experiments at future pp colliders like the LHC or the SSC, where a short data acquisition time is required because of the frequent bunch crossings and the high luminosity.

The work described in this paper was purely exploratory. We did not try in any way to improve the observed performance, for example by shaping the calorimeter signals. The results were strongly affected by the long, poor-quality signal cables (65 ns risetime in the response to a step function) used in these measurements. Since such cables can be avoided in a realistic application of this detector in an LHC/SSC environment, we measured their effect on the signals and unfolded it from the experimental results, if and when possible.

The calorimeter produces very fast signals. After (before) unfolding the mentioned cable effects, 90% of the charge is collected in 37 (80) ns for electromagnetic showers and in 47 (90) ns for hadronic ones. The performance remains practically unaffected for gates as short as 40 ns, even when the cable effects are not unfolded. When the gate width is reduced below this value, the effects of the truncated charge collection become measurable. The energy resolution gets worse, especially for hadrons. The e/π signal ratio increases, which causes a signal alinearity for hadronic showers. The hadronic shower profiles become narrower, causing a degradation of the electron/pion separation capability.

For a charge collection time of 16 ns (equivalent to the LHC/SSC bunch spacing), we found that the electromagnetic energy resolution deteriorated by about 50% and the hadronic one by a factor two. The e/π signal ratio at 80 GeV increased by 15% (12% after unfolding the cable effects) and the hadronic signal alinearity amounted to 25% over an order of magnitude in energy. The effective radius of the hadronic showers was reduced by 10%. After (before) unfolding the cable effects, typically 75% (52%) of the charge produced by electromagnetic showers and 65% (45%) of the hadronic charge was collected in this short time span.

The signal speed of a calorimeter of this type is determined by the following factors:

- The physics of the shower development
- The response characteristics of the fibers
- The response characteristics of the PM and its associated electronics
- The signal cables and other elements in the data acquisition chain

The fact that rise times of $\sim$ 3 ns and pulse widths smaller than 10 ns (at 20% of the amplitude) have been measured for shower signals from this type of detector

demonstrates that it is intrinsically a very fast device, holding great promise for excellent performance even at gate widths as short as the LHC/SSC bunch spacing time. For reaching this goal, dedicated studies of all the factors listed above are needed. Such studies should particularly concentrate on the effects of the fibers, since the choice of the fiber type might very well be dictated by factors other than the speed of response. It is well known that some relatively slow (green) fibers offer superior characteristics in terms of radiation hardness and light attenuation. Also, the absolute photoelectron yield achievable with the fiber/light detector combination might be an issue, in view of the e.m. energy resolution. In any case, such studies should be done with short, high-quality signal cables, thus avoiding the systematic effects encountered in the measurements described in this paper.

Acknowledgements

We are deeply grateful to the LAA Project Leader, Prof. A. Zichichi, for his vision, his warm interest and his encouraging support. We thank our colleagues from the UA2 Group, and in particular P. Jenni and L. Mapelli, who helped us in many ways, in particular during the beam tests. The work described in this paper would have been impossible without the outstanding technical support provided by our technicians O. Barnaba, C. Baudoin, M. Borriello, S. Bricola, J.-M. Chapuis, C. Farella, B. Foligne, A. Freddi, G. Improta, G. Iuvino, F. Pagano, S. Robinson, R. Rocco, L. Rose-Dulcina, G. Sannier, C. Schillinger, A. Sigrist and V. Vanzanella. Financial support from the Stichting for Fundamenteel Onderzoek der Materie to the NIKHEF group, from the Istituto Nazionale di Fisica Nucleare to the Cagliari, Napoli and Pavia groups, from the Junta Nacional de Investigação Científica of Portugal to the Lisbon group, from the Conselho Nacional de Desenvolvimento Cientifico e Tecnologico of Brazil to the Rio de Janeiro group, and from the U.S. Department of Energy and National Science Foundation to the San Diego group is acknowledged. Two of us (S.B. and F.R.) wish to thank the Digital Equipment Corporation for support. And finally, we are grateful to the staff of the SPS, and in particular to N. Doble, for the excellent beam conditions and assistance provided during our tests.

REFERENCES

1. G. Jarlskog and D. Rein (eds.), Proc. Large Hadron Collider Workshop, Aachen 1990, Vols. I,II,III, CERN 90-10/ECFA 90-133.
2. B. Aubert *et al.* (RD3 Collaboration), Performance of a Liquid Argon Electromagnetic Calorimeter with an 'Accordion' Geometry, preprint CERN-PPE/91-73 (1991).
3. R. DeSalvo *et al.*, Nucl. Instr. and Meth. **A279** (1989) 467.
4. D. Acosta *et al.*, Nucl. Instr. and Meth. **A294** (1990) 193.
5. D. Acosta *et al.*, Nucl. Instr. and Meth. **A302** (1991) 36.
6. D. Acosta *et al.*, Nucl. Instr. and Meth. **A305** (1991) 55.
7. D. Acosta *et al.*, Effects of radiation damage on scintillating fibre calorimetry, preprint CERN-PPE/91-45 (1991), to be published in Nucl. Instr. and Meth. B.
8. D. Acosta *et al.*, Nucl. Instr. and Meth. **A308** (1991) 481.
9. D. Acosta *et al.*, Nucl. Instr. and Meth. **A309** (1991) 143.
10. T. Åkesson *et al.*, Nucl. Instr. and Meth. **A262** (1987) 243.
11. R. Wigmans, Nucl. Instr. and Meth. **A259** (1987) 389.
12. E. Bernardi *et al.*, Nucl. Instr. and Meth. **A262** (1987) 229.
13. We define the *nuclear interaction length* λ_I in the same way as the Particle Data Group in Phys. Lett. **B239** (1990), page III 5,6. It is the mean free path for *protons* between inelastic interactions. We use the symbol λ_π for pions. Since the inelastic cross sections for protons are 50% larger than for pions, $\lambda_\pi \approx 1.5\lambda_I$.
14. See for example: N.S. Nahman and R.L. Wigington, Proc. of the IRE (1957) 166; G. Amsel *et al.*, Rev. Scient. Instr. **42** (1971) 1237.
15. J.M. Seixas, L.P. Calôba and M.N. Souza, Application of Signal Processing Techniques on the Analysis of a Lead/Scintillating-Fiber Calorimeter in Short Acquisition Time Environments, report CERN-PPE/91-165, CERN, Geneva (1991).
16. H. Abramowicz *et al.*, Nucl. Instr. and Meth. **180** (1981) 429.
17. D. Acosta *et al.*, Lateral Shower Profiles in a Scintillating Fiber Calorimeter, in preparation.

FIGURE CAPTIONS

1. Detail of the front face of the calorimeter (a) and the lateral structure of the detector as a whole (b).
2. The handling of the photomultiplier signals. See text for details.
3. Layout of the beam line. See text for details
4. Results of measurements and simulations of the effects of the signal cables on fast pulses. The step function generated by a pulse generator (a). The measured response to this step function after it has travelled through a 100 m long coaxial signal cable (b). The same response after unfolding the cable effects (c). See text for details.
5. Scatter plots of the calorimeter signals from 80 GeV pions entering the detector in the center and measured in the fourth hexagonal ring. The ring sum signals (vertical) are plotted versus the ones obtained by summing the signals from the 24 individual towers constituting this ring. Results for gate widths of 358 ns (a) and 15 ns (b).
6. Scatter plots of the calorimeter signals from 80 GeV pions entering the detector in the center and measured in the first (a, b) and fourth (c, d) calorimeter ring. The amplified signals (vertical) are plotted versus the unamplified ones. Results for gate widths of 358 ns (a, c) and 15 ns (b, d).
7. The calorimeter signal as a function of the time during which the charge is integrated by the ADC. The results are normalized to the ones obtained for 358 ns. The measured data are shown in (a); after correcting for the effects of the signal cables, the results shown in (b) were obtained. Results for 80 GeV electrons and pions entering the central tower of the calorimeter at $\theta_z = 3^0$.
8. The calorimeter signal as a function of the time during which the charge has been collected, based on sampling measurements with a digitizing oscilloscope. Data for 80 GeV electrons and pions entering the central tower of the calorimeter at $\theta_z = 3^0$. The signals concern the central 7 towers of the detector. The (small) effects of the signal cable are unfolded.
9. The energy resolution for 80 GeV electrons, entering the calorimeter at $\theta_z = 3^0$, as a function of the charge collection time. The results are normalized to the resolution for a 358 ns gate. Both the resolutions obtained from a Gaussian fit to the signal distribution and σ_{RMS} are shown.
10. Signal distributions for 80 GeV electrons, measured for a 358 ns gate (a) and for a 15 ns gate (b). The curves are the result of Gaussian fits.
11. The energy resolution for 80 GeV pions, entering the calorimeter at $\theta_z = 3^0$, as a function of the charge collection time. The results are normalized to the resolution

for a 358 ns gate. Both the resolutions obtained from a Gaussian fit to the signal distribution and σ_{RMS} are shown.

12. The energy resolution for pions as a function of the energy, plotted on a scale linear in $E^{-1/2}$, for gate widths of 16 and 358 ns. The energy resolutions are the results of Gaussian fits to the signal distributions. No correction for the effects of light attenuation was made.

13. The e/π signal ratio for 80 GeV particles as a function of the gate width. The data are normalized to the value obtained for a 358 ns gate. Both the results obtained before and after unfolding the effects of the signal cables are shown.

14. The ratio of the calorimeter signals for pions at gate widths of 16 and 358 ns, as a function of the energy.

15. Lateral shower profiles of 80 GeV pions entering the central calorimeter tower at an angle $\theta_z = 3^0$, measured for gate widths of 358 ns and 20 ns. The curves are the results of fits to expression (1). See text for details.

16. The ratio E/G, describing the relative contribution of the shower tail to the signal, as a function of the charge collection time. Shown are the results of fits to the shower profiles before and after unfolding the cable effects.

17. The e/π signal ratio at 80 GeV as a function of the radius of the area around the shower axis over which the calorimeter signals are integrated, for various values of the charge collection time.

18. The e/π signal ratio as a function of the charge collection time for two different cluster sizes. The signals are integrated over an area with a radius of 24 or 49 cm around the impact points of the particles. The e/π ratios for these two data sets are separately normalized to the values for a 358 ns gate.

19. The pion rejection factor, normalized to the one for a 358 ns gate, as a function of the charge collection time. These results were obtained from an analysis of e/π separation through the differences in the lateral shower profile. This pion rejection factor was found by comparing the effective radius R of pion showers with the R value for which the electron efficiency equals 99%. Data for 80 GeV particles.

20. The pion rejection factor, normalized to the one for a 358 ns gate, as a function of the charge collection time. The pion rejection factor was obtained from an analysis of the width (FWFM) of the shower pulses. Shown are the results for the measured pulses and for the ones sent through a digital filter that eliminates the effects of RC components in the data acquisition chain. The curves are drawn to guide the eye. Data for 80 GeV and an electron efficiency of 98%.

TABLE CAPTIONS

1. The fraction of the shower charge collected for different values of the gate width, before and after unfolding the effects of the 100 m long signal cables. Data for 80 GeV electromagnetic and hadronic showers.
2. The time needed to collect 90% of the charge from different signals, measured either with the charge ADC's or with the sampling oscilloscope. Results are given before and after unfolding the effects of the cables used in these measurements.
3. The electromagnetic and hadronic energy resolution for different charge collection times. The resolutions (σ/E) are normalized to the values obtained for a 358 ns gate. The values for σ are either the RMS values taken from the signal distribution (RMS columns) or the results of a Gaussian fit (Gauss columns). Data for 80 GeV electrons and pions at $\theta_z = 3^0$.
4. The e/π signal ratio at 80 GeV for different charge collection times. Listed are the actual values of the measured signal ratio and the values normalized to the e/π signal ratio at a 358 ns gate, before and after unfolding the effects of the 100 m long signal cables.
5. The parameters B_1, B_2, λ_1 and λ_2 of the hadronic shower profile induced by 80 GeV pions at $\theta_z = 3^0$ (1), and the ratio E/G of the contributions of the exponential and Gaussian components to the calorimeter signal (2), for different values of the charge collection time. Listed are the values obtained before/after unfolding the effects of the 100 m long signal cables.

Table 1 The fraction of collected charge				
Gate (ns)	e measured (%)	e unfolded (%)	π measured (%)	π unfolded (%)
358	100	100	100	100
251	98.7	100.0	99.4	100.0
154	96.0	100.0	95.7	99.5
108	91.6	99.4	91.1	98.1
58	83.4	94.7	81.9	92.8
39	75.3	90.2	72.6	87.0
30	68.6	86.5	64.4	82.2
25	64.9	83.7	59.7	78.5
20	58.9	80.1	53.0	73.7
15	52.3	75.4	45.2	67.6
10	42.3	69.0	34.4	59.4
5	27.5	60.3	19.6	47.2

Table 2 Rise times (90% charge collection)		
Type of signal	ADC measurement (ns)	Scope measurement (ns)
Step function measured	65	6
Step function unfolded	2	< 1
80 GeV e^- measured	80	36
80 GeV e^- unfolded	37	31
80 GeV π^- measured	90	42
80 GeV π^- unfolded	47	37

Table 3 The energy resolution				
Gate (ns)	$\sigma^{e}_{\mathrm{RMS}}$	$\sigma^{e}_{\mathrm{Gauss}}$	$\sigma^{\pi}_{\mathrm{RMS}}$	$\sigma^{\pi}_{\mathrm{Gauss}}$
358	1	1	1	1
251	0.995±0.034	0.964±0.033	1.015±0.024	1.030±0.024
154	0.973±0.036	0.927±0.034	1.000±0.025	1.043±0.026
108	1.031±0.034	0.981±0.032	1.023±0.025	1.067±0.026
58	0.968±0.033	0.936±0.032	1.077±0.024	1.062±0.024
39	1.057±0.035	0.972±0.032	1.207±0.026	1.121±0.024
30	1.095±0.035	1.048±0.033	1.300±0.028	1.182±0.025
25	1.120±0.038	1.069±0.036	1.394±0.030	1.249±0.027
20	1.301±0.045	1.168±0.040	1.425±0.029	1.300±0.026
15	1.485±0.047	1.194±0.038	1.596±0.036	1.496±0.034
10	2.270±0.072	1.670±0.053	2.053±0.047	1.917±0.044

Table 4 The e/π signal ratio (80 GeV)			
Gate (ns)	e/π measured	$[e/\pi]/[e/\pi]_{t=358ns}$ measured	$[e/\pi]/[e/\pi]_{t=358ns}$ unfolded
358	1.013 ± 0.001	1	1
154	1.016 ± 0.002	1.003 ± 0.002	1.005 ± 0.002
108	1.019 ± 0.002	1.006 ± 0.002	1.014 ± 0.002
58	1.032 ± 0.002	1.019 ± 0.002	1.021 ± 0.002
39	1.052 ± 0.002	1.039 ± 0.002	1.036 ± 0.002
30	1.077 ± 0.002	1.063 ± 0.002	1.053 ± 0.002
25	1.102 ± 0.002	1.088 ± 0.002	1.067 ± 0.002
20	1.127 ± 0.002	1.113 ± 0.002	1.087 ± 0.002
15	1.172 ± 0.003	1.157 ± 0.003	1.115 ± 0.003
10	1.247 ± 0.004	1.231 ± 0.005	1.161 ± 0.005

Table 5 The hadronic shower profile

Gate (ns)	B_1	λ_1 (cm)	B_2	λ_2 (cm)	E/G
358	1.62 / 1.65	14.6 / 14.4	7.2 / 7.0	4.50 / 4.68	0.815 / 0.823
251	1.63 / 1.67	14.5 / 14.3	7.2 / 7.1	4.51 / 4.48	0.848 / 0.820
154	1.61 / 1.60	14.6 / 14.2	7.2 / 6.9	4.54 / 4.50	0.834 / 0.811
108	1.50 / 1.58	14.2 /14.6	6.7 / 7.1	4.45 / 4.55	0.808 / 0.800
58	1.49 / 1.34	14.3 / 14.0	6.9 / 6.0	4.54 / 4.49	0.783 / 0.768
39	1.37 / 1.16	14.1 / 14.2	6.5 / 5.4	4.52 / 4.51	0.753 / 0.740
30	1.27 / 1.02	14.0 / 13.9	6.2 / 5.0	4.52 / 4.45	0.725 / 0.714
25	1.19 / 0.94	14.0 / 13.7	6.0 / 4.7	4.52 / 4.48	0.694 / 0.698
20	1.10 / 0.82	14.0 / 13.4	5.9 / 4.3	4.52 / 4.44	0.658 / 0.653
15	0.95 / 0.60	14.2 / 14.5	4.3 /.3.8	4.52 / 4.47	0.578 / 0.640
10	0.83 / 0.46	13.8 / 14.2	4.7 / 3.0	4.46 / 4.38	0.562 / 0.620

APPENDIX A

Unfolding the cable effects

When a fast electronic signal is transmitted through a standard coaxial cable and electronic circuits, the signal shape is changed. Both the rise time and the decay time characteristics are affected. We have verified that the main effect on the signal shape comes from the 100 m long RG58 signal cables between the bases and the OLIFAN splitters (fig. 2). The long signal cables and their relatively poor quality had a considerable effect on the calorimeter signals. To unfold the effects of the cable, a procedure was developed, using methods from circuit theory[A1], to calculate the input signal as a function of time, given the measured output signal in the form of a series of current integrations obtained with a charge sensitive ADC for different gate lengths. To achieve this goal, it was necessary to find a mathematical representation of a system (to be called a compensating network or filter) that compensates for the effects of the cable. The cable/filter combination should pass the input signal unchanged, apart from a delay which is irrelevant.

Let us consider the signal cable as a system[A2] with an impulse response $h(t)$ (the response to a Dirac delta-function $\delta(t)$). When an input signal $p_1(t)$ (the photomultiplier signal) is transmitted through this cable, the resulting signal $p_2(t)$ at the end of the cable is described in the time domain by the convolution of the impulse response function of the cable and the input signal:

$$p_2(t) = \int_0^t h(t-x)p_1(x)dx \qquad (A1)$$

with the initial conditions $h(t) = p_1(t) = 0$. After applying a Laplace transform of $(A1)$ to the (complex) frequency domain, the convolution becomes a product:

$$P_2(s) = H(s)P_1(s) \qquad (A2)$$

The capital letters represent the Laplace transforms of the corresponding time dependent functions and s is the (complex) frequency[A3]. One can find $p_1(t)$ by constructing $H^{-1}(s)$ and performing the inverse Laplace transform on $H^{-1}(s)P_2(s)$.

We can write

$$H(s) = H_0(s)e^{-sT_0} \qquad (A3)$$

where the factor $\exp(-sT_0)$ represents the cable delay T and H_0 contains the remaining, more interesting information. The cable response $r(t)$ to a step function $u(t)$ was measured, neglecting the delay. The signal cable normally connected to the output of one of

the PM tubes was connected to the output of a pulse generator. The signal at the other end of the cable was measured with an oscilloscope (fig. 4b). The effects of the cable are seen to be considerable. The rise time, defined as the time interval Δt it takes to go from $r(t) = 10\%$ to $r(t + \Delta t) = 90\%$ of the final value, is 65 ns. In addition, the time it takes to go from 90% to 99% is a multiple of this number, so that the cable introduces very long tails to the signals. The response of the cable to the complementary function

$$c(t) = [1 - r(t)]u(t) \tag{A4}$$

turned out to be well described by the sum of three exponentials

$$c(t) = \sum_{i=1}^{3} a_i(t) e^{-\lambda_i t} \tag{A5}$$

When fitting the experimental data to this expression, the 6 parameters are constrained in a way described below. The time constants λ_i^{-1} are 2.2, 7.1 and 101 ns, respectively. The function $h(t)$ is related to the step response as

$$r(t) = \int_0^t h(x)dx \tag{A6}$$

The Laplace transform of this relation is

$$R(s) = H(s)/s \tag{A7}$$

Comparing this with the Laplace transform of the complementary function (A4)

$$C(s) = \frac{1}{s} - R(s) \tag{A8}$$

we find that

$$H(s) = 1 - sC(s) \tag{A9}$$

Since the Laplace transform of $e^{-\lambda t}$ is $1/(s + \lambda)$, $H_0(s)$ becomes

$$H_0(s) = \frac{s + 0.012}{(s + 0.46)(s + 0.14)(s + 0.0099)} \tag{A10}$$

with s in Grad/s. The constraints mentioned above have been chosen in such a way that the numerator in (A10) has two powers of s less than the denominator. The inverse $H_0^{-1}(s)$ is now simply the algebraic inverse of $H_0(s)$ given in (A10).

We interpret $H_0^{-1}(s)$ by using the impulse invariance method of ref. A2. We introduce parasitic poles in $(A10)$ by multiplying it by

$$\frac{\sigma_{p_1}\sigma_{p_2}}{(s+\sigma_{p_1})(s+\sigma_{p_2})}$$

with the assumption that $\sigma_{p_i} \gg s$. This assumption corresponds to cutoffs at extremely high frequencies well beyond the region of interest. Thus $H_0(s)$ is written as a product of three factors, each of the form

$$\frac{s+\sigma_z}{s+\sigma_p} = 1 + \frac{\sigma_z - \sigma_p}{s+\sigma_p} \tag{A11}$$

We now make a transformation to the $\mathcal{Z}$ domain. Equation $A11$ leads then to

$$V_2(z) = (\sigma_z - \sigma_p)TV_1(z) + \alpha z^{-1}V_2(z) \tag{A12}$$

or

$$\frac{V_2(z)}{V_1(z)} = \frac{(\sigma_z - \sigma_p)T}{1 - \alpha z^{-1}} \tag{A13}$$

where $V_i(z)$ represents the $z-$transform of the discrete-time function $v_i(nT)$. In circuit theory terminology we can represent $(A11)$ by a circuit with a feedback loop: The term $(\sigma_z - \sigma_p)T$ represents an amplification of the input signal, with T the sampling period (1 ns in our case). A fraction α of the output signal is added to the input signal through the feedback loop. The denominator of the second term in $(A11)$ represents a factor $\exp(-\sigma_p t)$ in the time domain and therefore $\alpha = \exp(-\sigma_p T)$, as required by the impulse invariance method. The feedback loop has a time delay represented by z^{-1}. From the pole in $(A13)$ we find $z_p = \alpha = \exp(-\sigma_p T)$. We have so far considered only the second term in $(A11)$. Including the first term, $(A12)$ becomes

$$V_2(z) = V_1(z) + (\sigma_z - \sigma_p)TV_1(z) + \alpha z^{-1}V_2(z) \tag{A14}$$

In this equation $(\sigma_z - \sigma_p)T$ is dimensionless while the factor z^{-1} corresponds to a delay in the time domain. We can therefore write $(A14)$ in the form of a recursive difference equation

$$v_2(n) = v_1(n) + (\sigma_z - \sigma_p)Tv_1(n) + \alpha v_2(n-1) \tag{A15}$$

with n the step number, labeling time in units of T. This procedure is repeated three times, once for each of the three factors of the form $(A11)$ in H_0^{-1} with the initial conditions $v_1(t) = v_2(t) = 0$ for $t < 0$.

In preparation for the actual unfolding of the integrated photomultiplier signals, the measured charges as function of the ADC gate widths (see fig. 7a) were used to define complementary signals in analogy with ($A4$). The complementary signals were fitted to the sum of three exponentials

$$p_2(t) = \sum_{i=1}^{3} b_i(t) e^{-\nu_i t} \qquad (A16)$$

Unlike in ($A5$) no constraints were applied to the 6 parameters. The validity of this method was checked with the response to the step function measured before. After unfolding the cable effects in the way described, the rise time was reduced from 65 ns to 6 ns. After a second iteration in which the unfolded curve was processed in the same way, the rise time became 2 ns. This is illustrated in fig. 4c. To improve further upon these results it would be necessary to also unfold the effects of the electronic circuits such as the OLIFAN and the linear adders since these effects are comparable. But since the risetime of the SPACAL pulses amounts anyway to $\sim 2-3$ ns, such a degree of detail is not really useful.

The described procedure introduces inevitably some uncertainties in the experimental results. For example, the description of the step response by the sum of three exponential functions ($A5$) is purely empirical and therefore rather arbitrary. However, the fact that the unfolded experimental results agree reasonably well with results obtained independently with much faster cables (see e.g. Table 2) gives us some confidence in the validity of the method.

References:

[A1] J.M. Seixas, L.P. Calôba and M.N. Souza, A Simple Method for Cable Compensation with fast Pulse Transmission Applications, report CERN-PPE/91-84, CERN, Geneva (1991).

[A2] A.V. Oppenheim and R.W. Schafer, Discrete-Time Signal Processing, Prentice-Hall, 1989.

[A3] A.V. Oppenheim, A.S. Willsky and I.T. Young, Signals and Systems, Prentice-Hall, 1983.

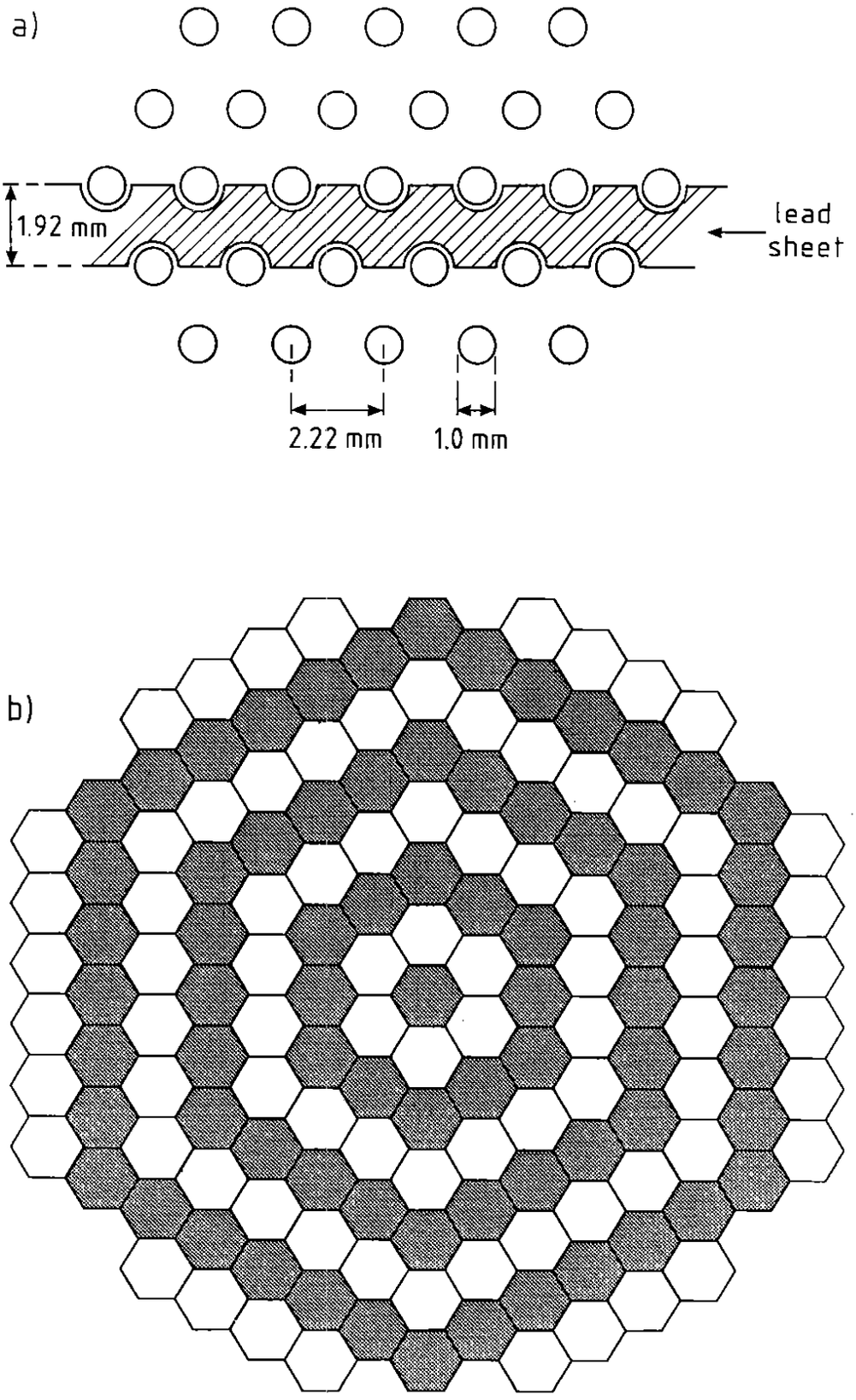

Figure 1

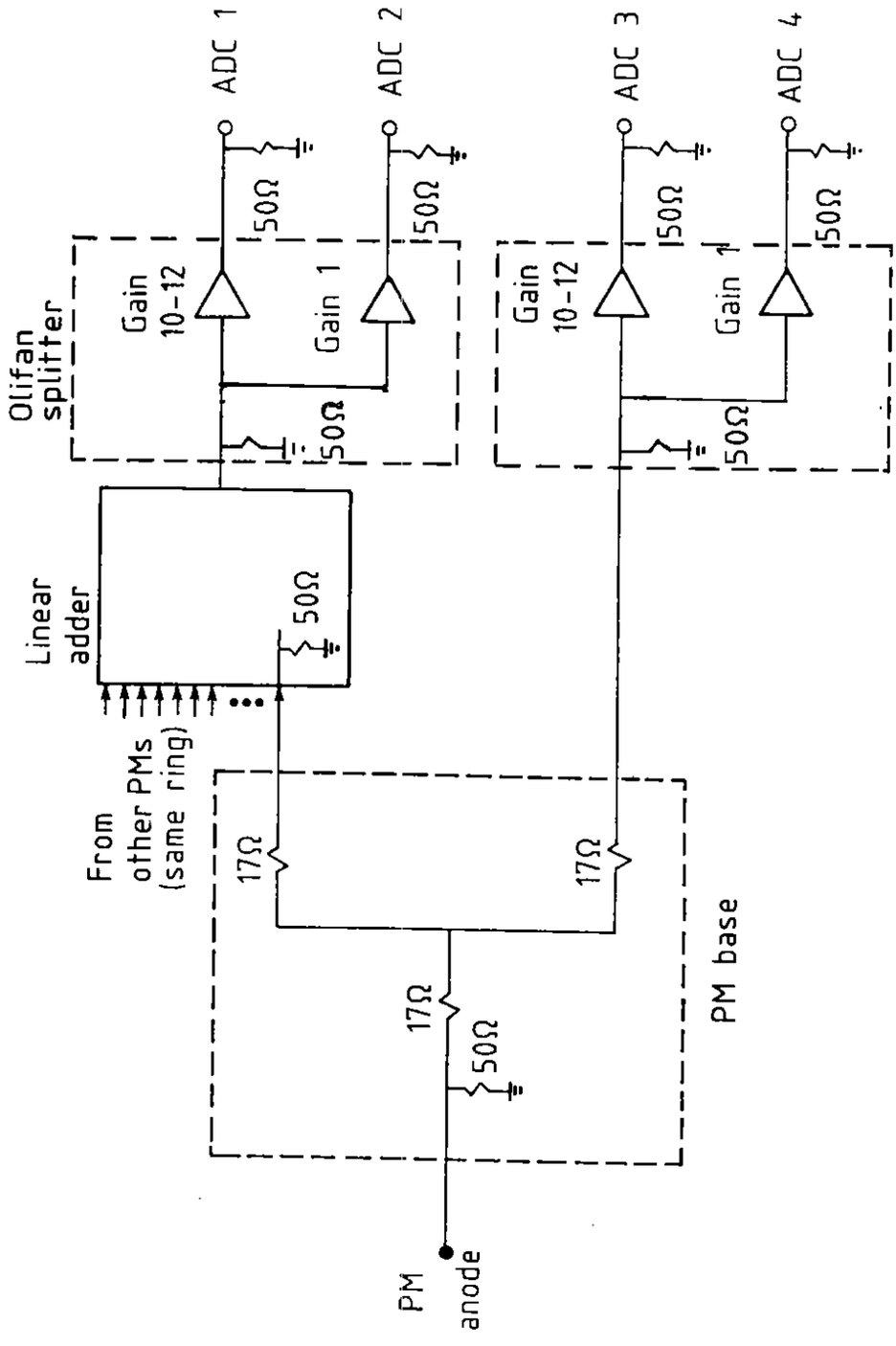
ADC 1
ADC 2
ADC 3
ADC 4
50Ω
Olifan splitter
Gain 10-12
Gain 1
Linear adder
From other PMs (same ring)
17Ω
PM base
PM anode

Figure 2

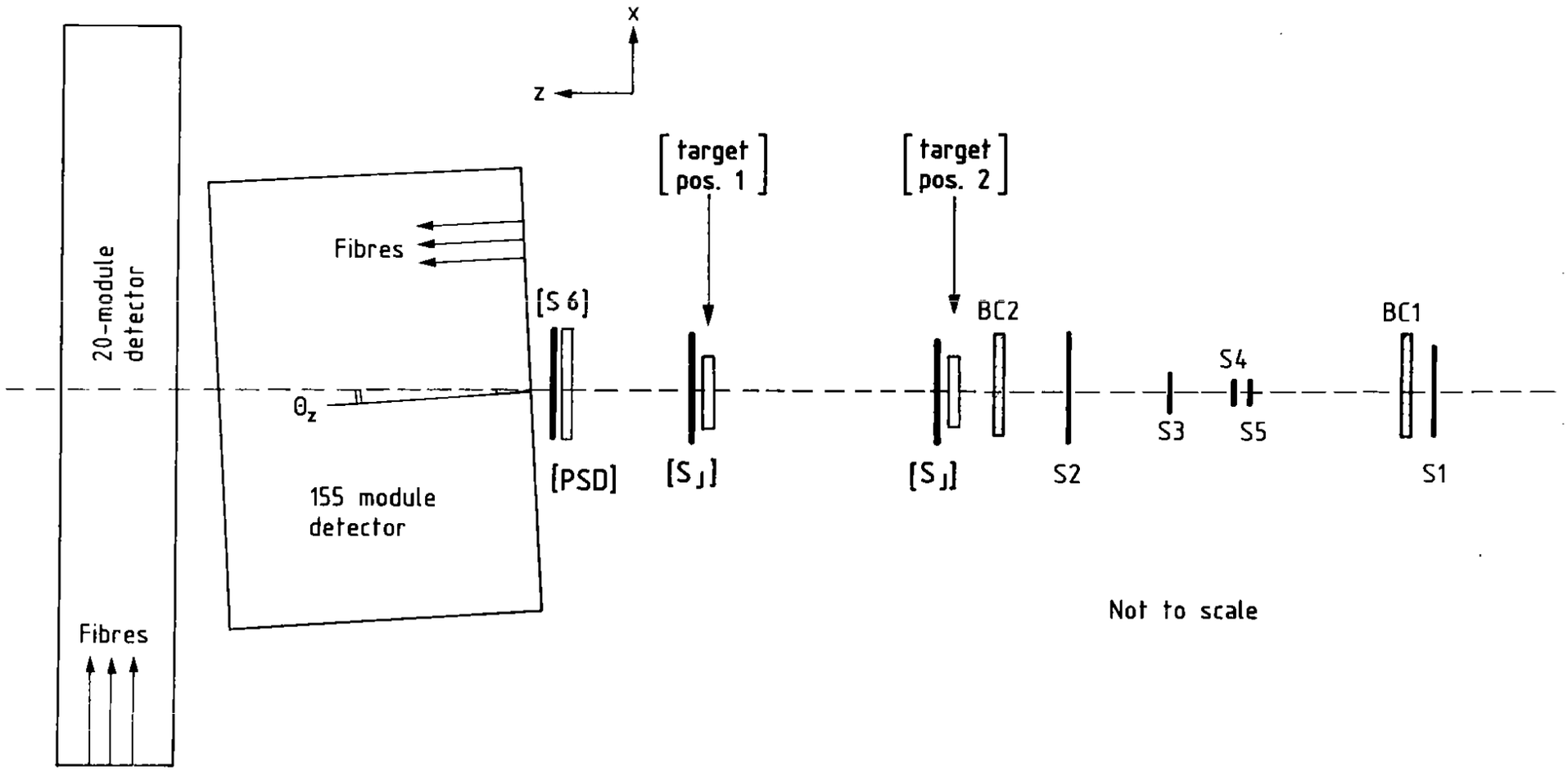
x
z
20-module detector
Fibres
155 module detector
Fibres
θ_z
[S 6]
[PSD]
[target pos. 1]
[S_J]
[target pos. 2]
[S_J]
BC2
S2
S3
S4
S5
BC1
S1
Not to scale

Figure 3

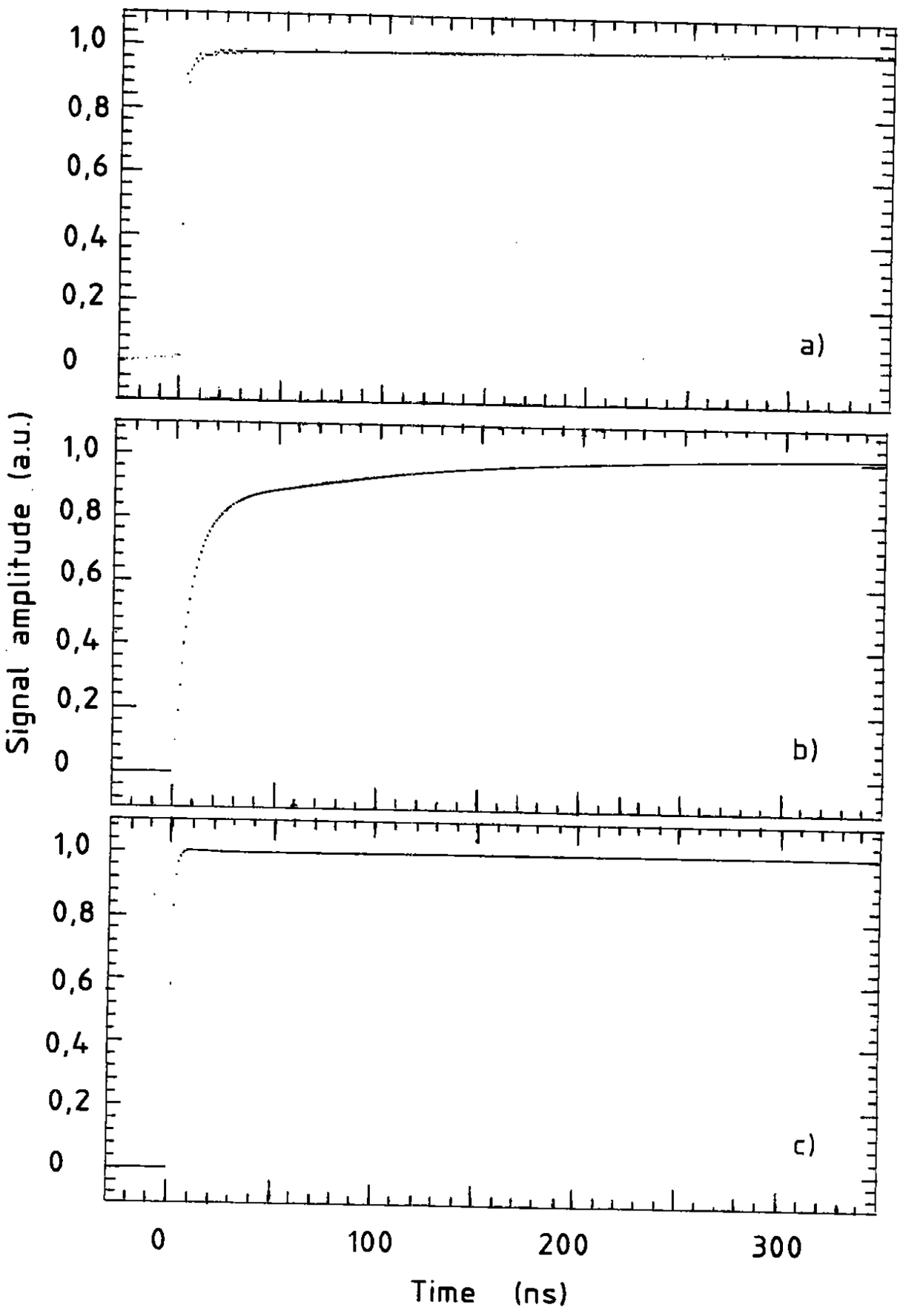

Figure 4

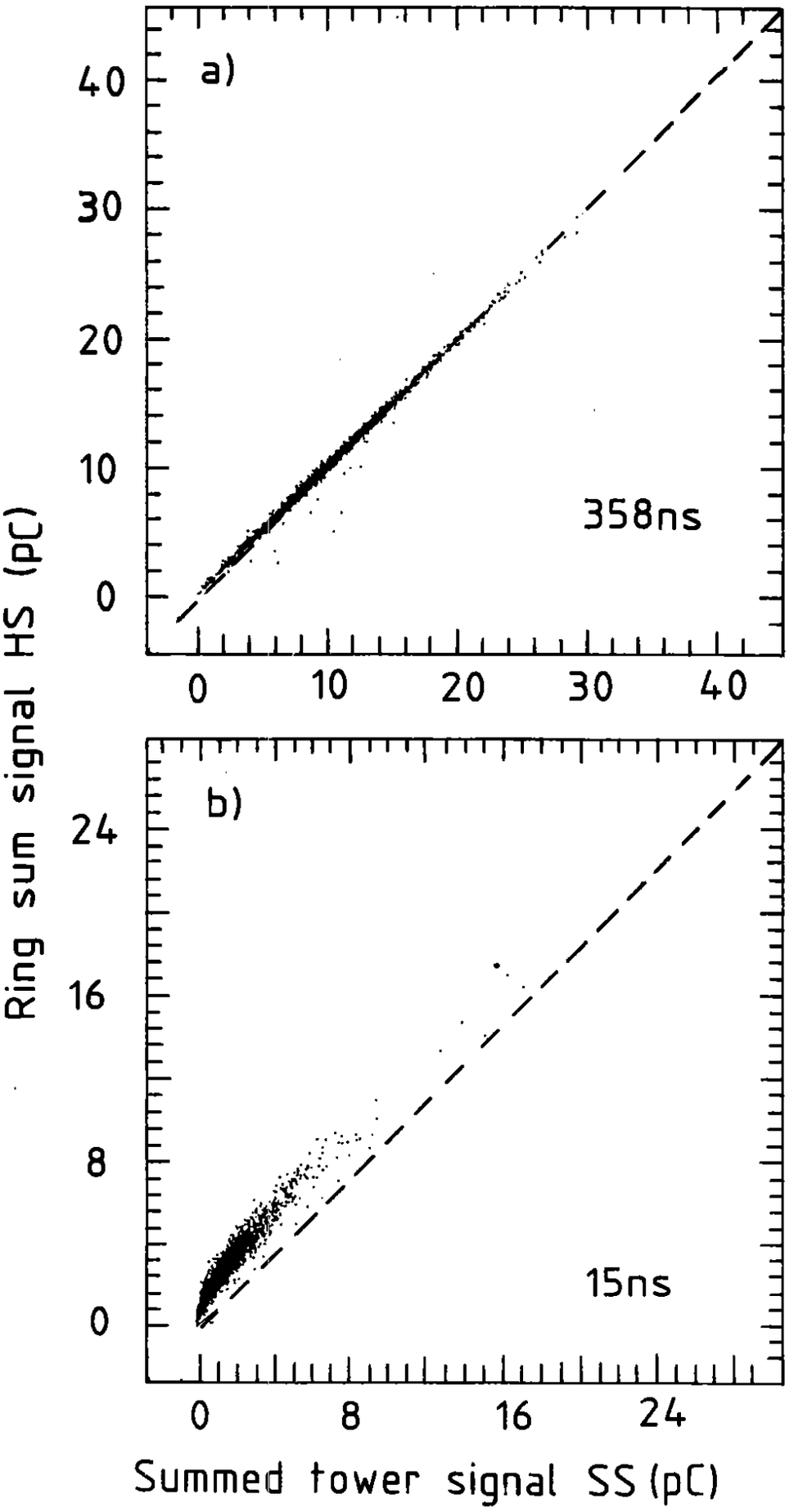
a)
40
30
20
10
0
358ns
0
10
20
30
40
b)
24
16
8
0
15ns
0
8
16
24
Ring sum signal HS (pC)
Summed tower signal SS (pC)

Figure 5

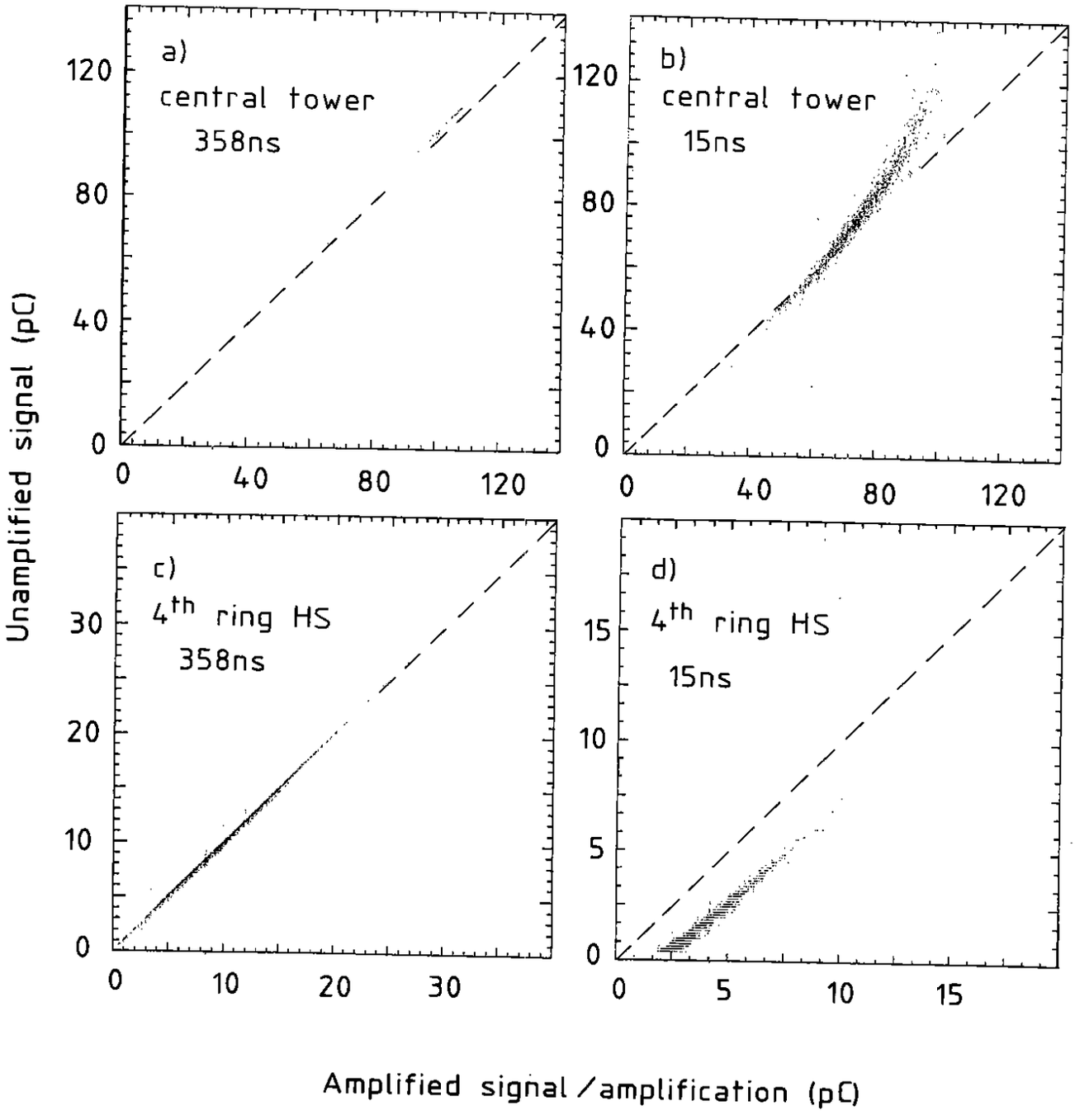
a)
central tower
358ns
b)
central tower
15ns
c)
4th ring HS
358ns
d)
4th ring HS
15ns
Unamplified signal (pC)
Amplified signal / amplification (pC)
0
40
80
120
10
20
30
5
15

Figure 6

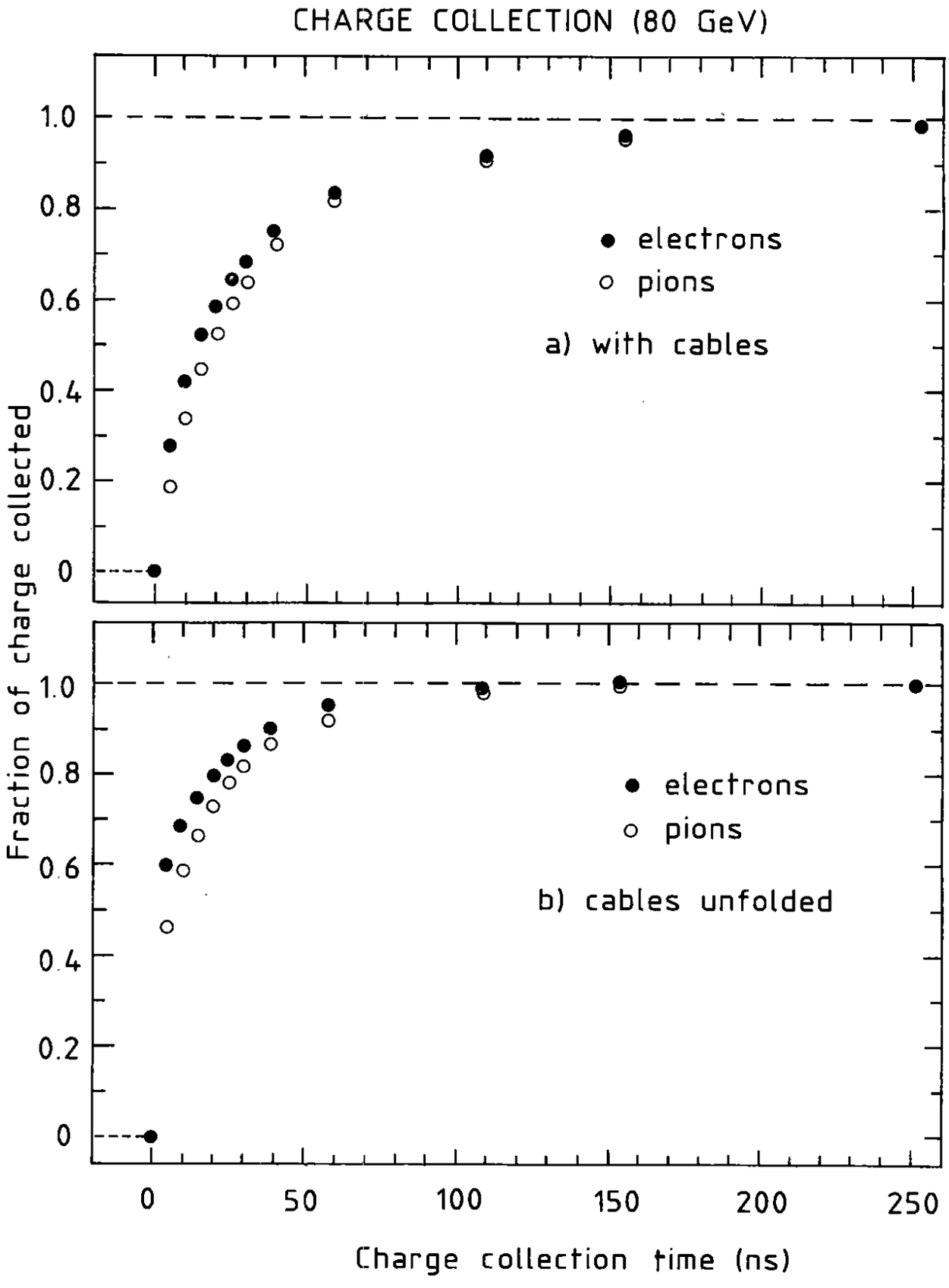
CHARGE COLLECTION (80 GeV)
Fraction of charge collected
1.0
0.8
0.6
0.4
0.2
0
electrons
pions
a) with cables
b) cables unfolded
0
50
100
150
200
250
Charge collection time (ns)

Figure 7

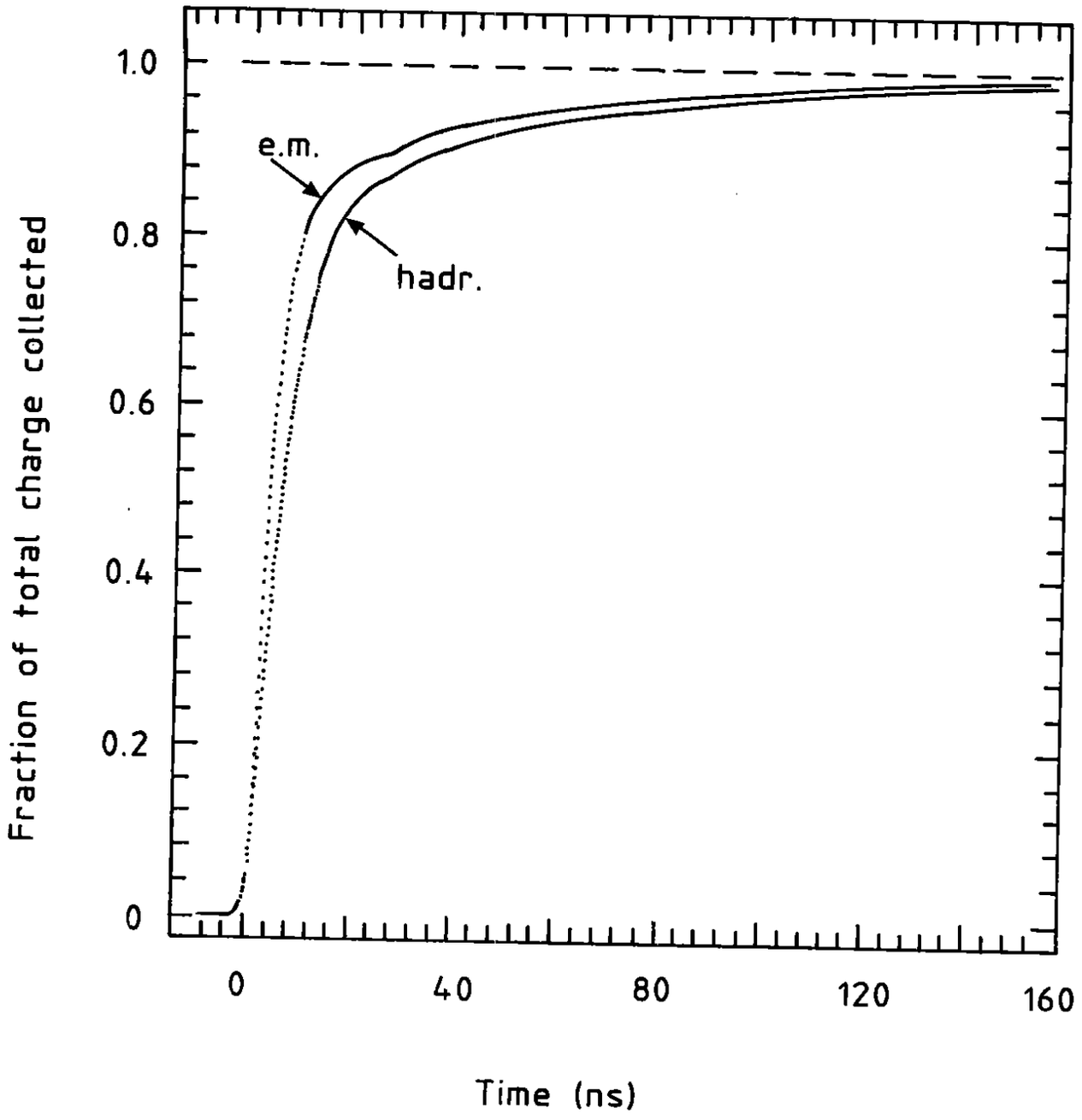
1.0
0.8
0.6
0.4
0.2
0
e.m.
hadr.
Fraction of total charge collected
0
40
80
120
160
Time (ns)

Figure 8

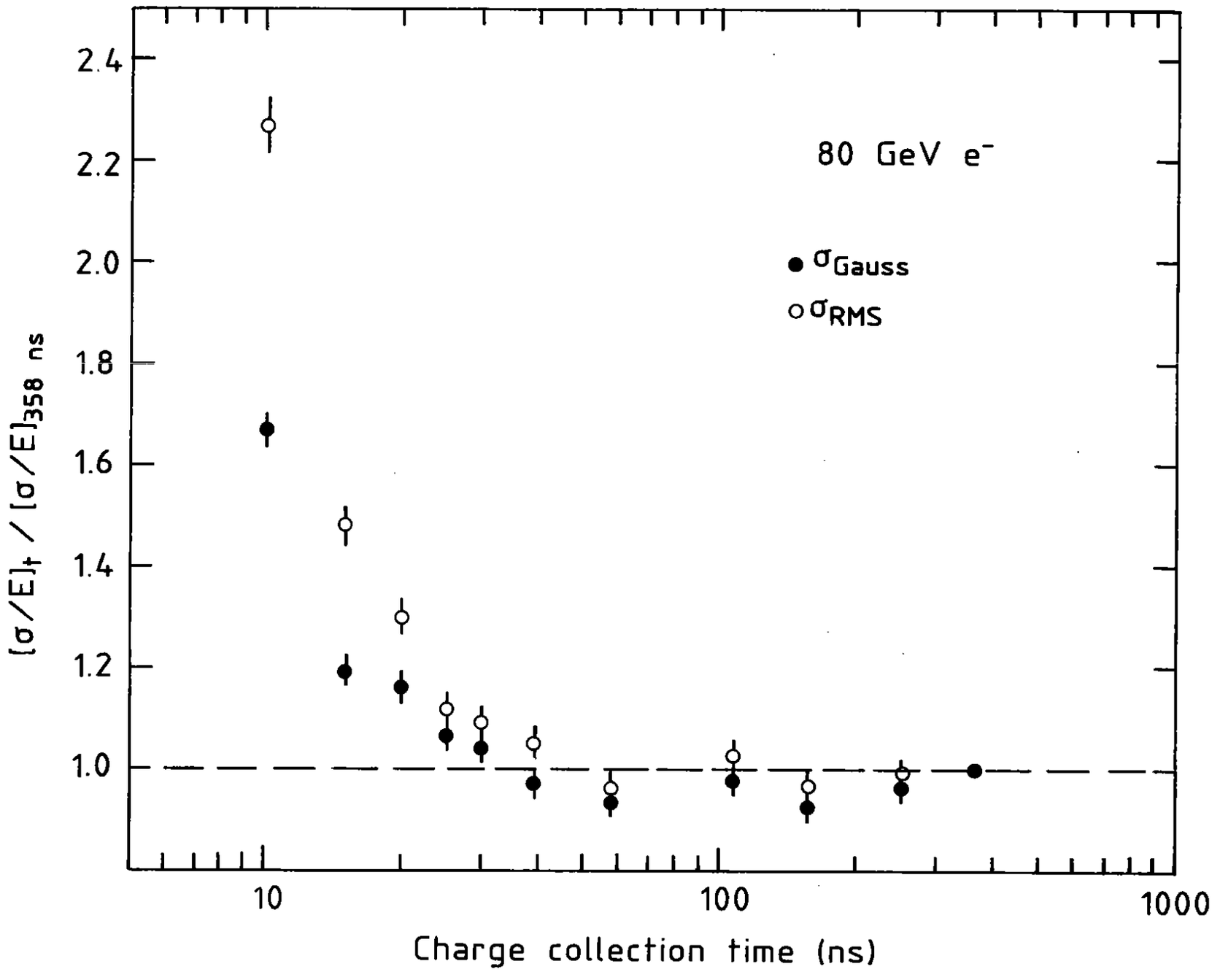
80 GeV e⁻
σGauss
σRMS
[σ/E]t / [σ/E]358 ns
Charge collection time (ns)
2.4
2.2
2.0
1.8
1.6
1.4
1.2
1.0
10
100
1000

Figure 9

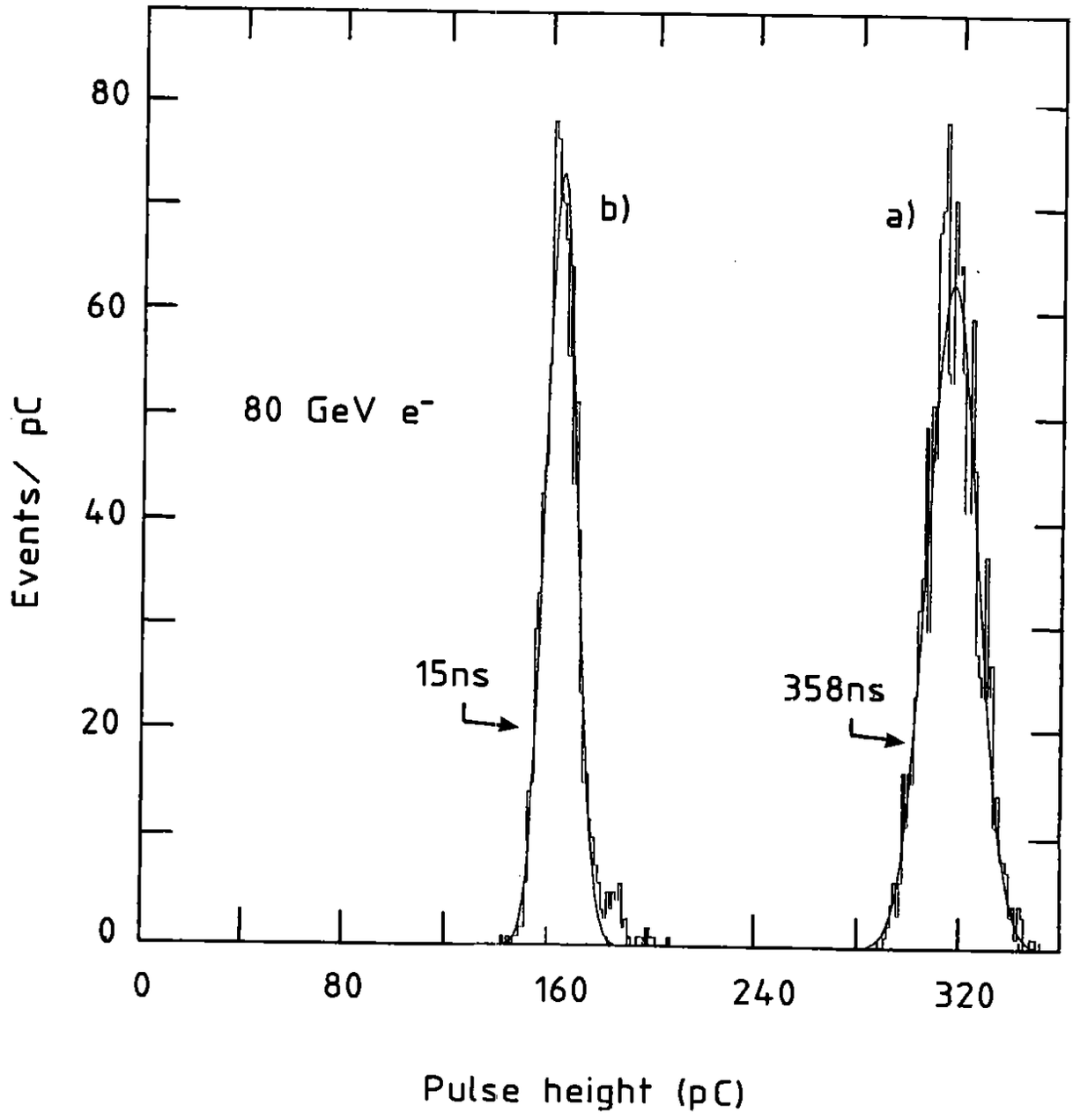
80
60
40
20
0
Events/ pC
80 GeV e⁻
b)
a)
15ns
358ns
0
80
160
240
320
Pulse height (pC)

Figure 10

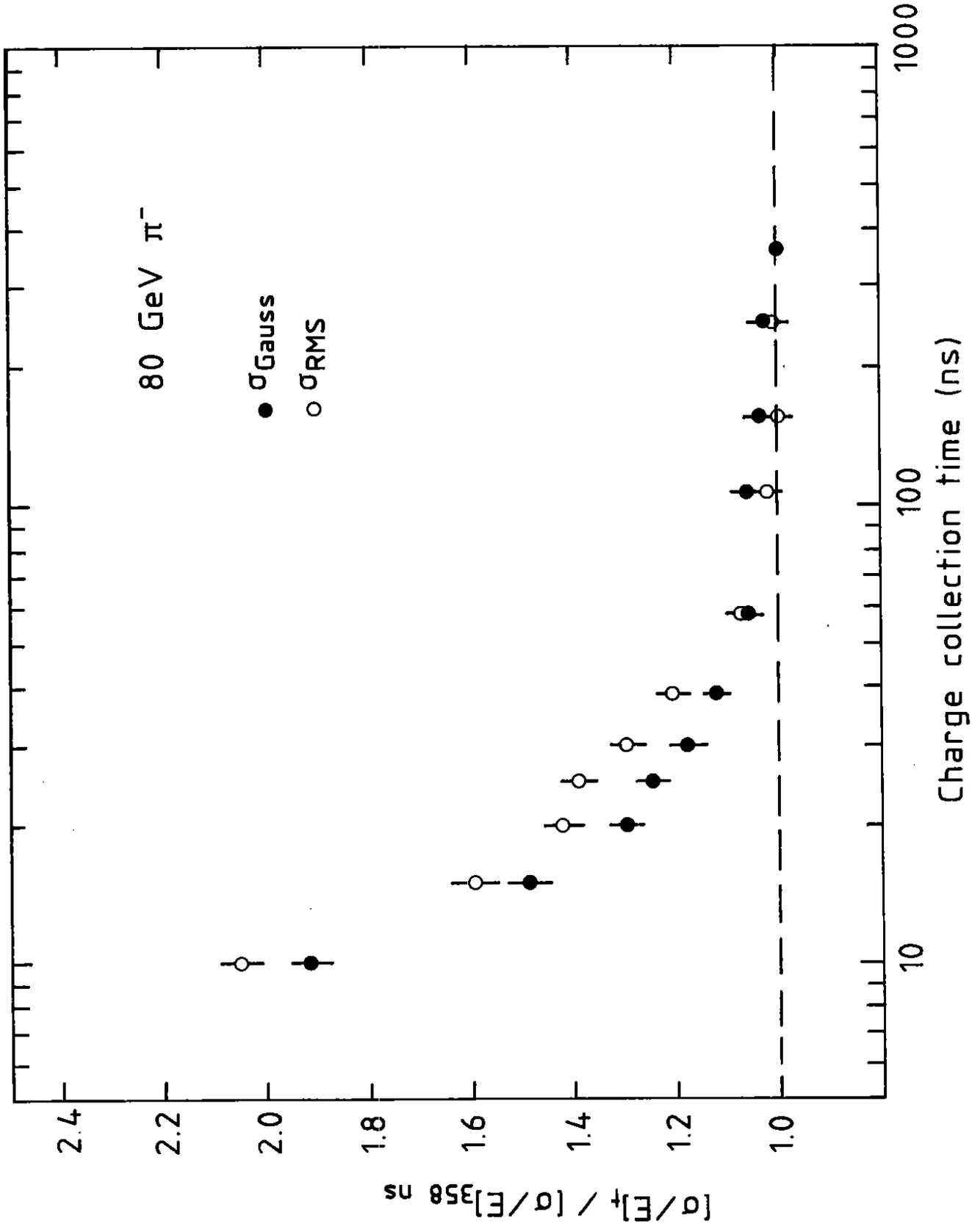
80 GeV π⁻
σGauss
σRMS
[σ/E]t / [σ/E]358 ns
Charge collection time (ns)
2.4
2.2
2.0
1.8
1.6
1.4
1.2
1.0
10
100
1000

Figure 11

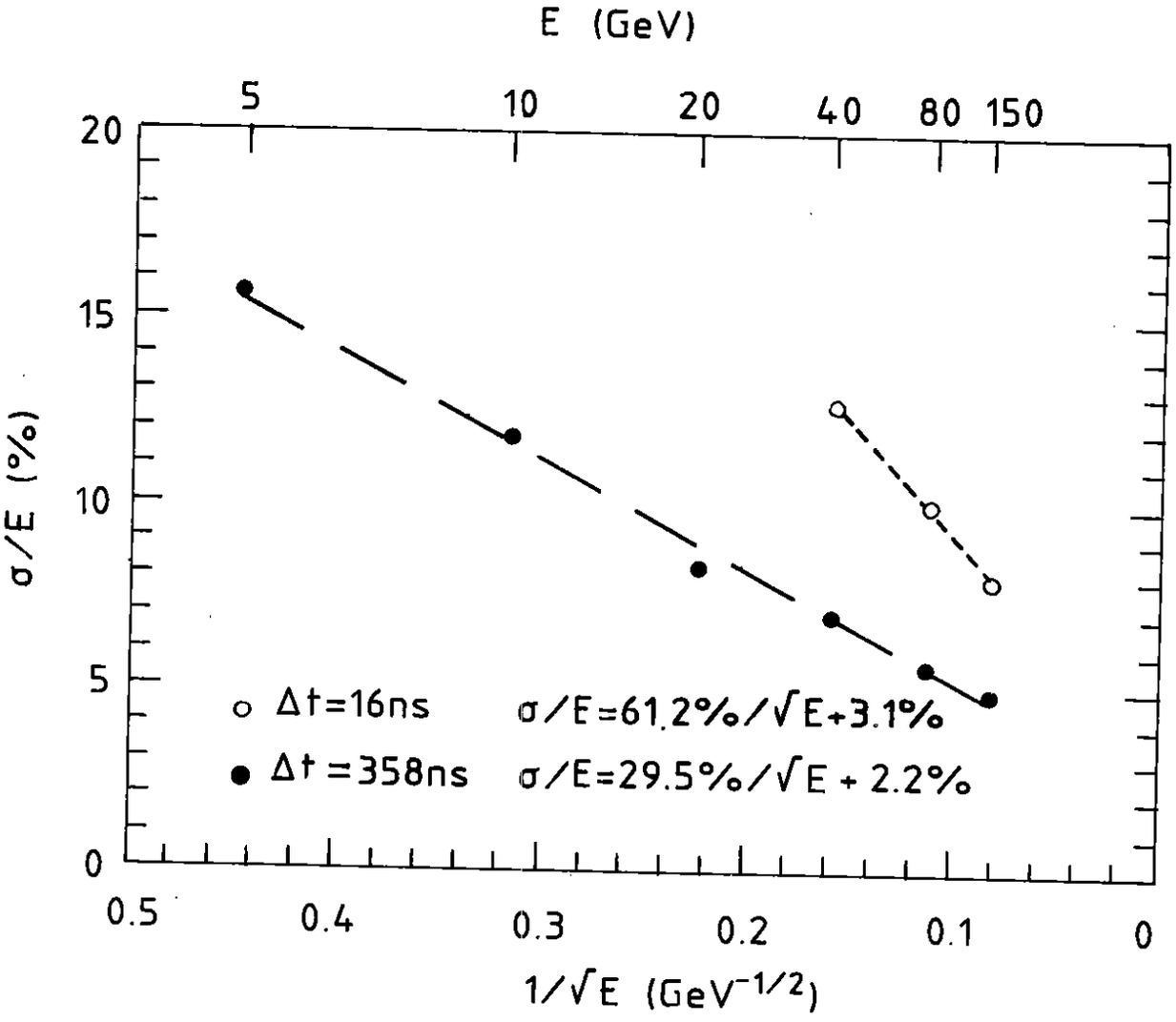
E (GeV)
5
10
20
40
80
150
20
15
10
5
0
σ/E (%)
Δt=16ns
σ/E=61.2%/√E+3.1%
Δt=358ns
σ/E=29.5%/√E + 2.2%
0.5
0.4
0.3
0.2
0.1
0
1/√E (GeV^-1/2)

Figure 12

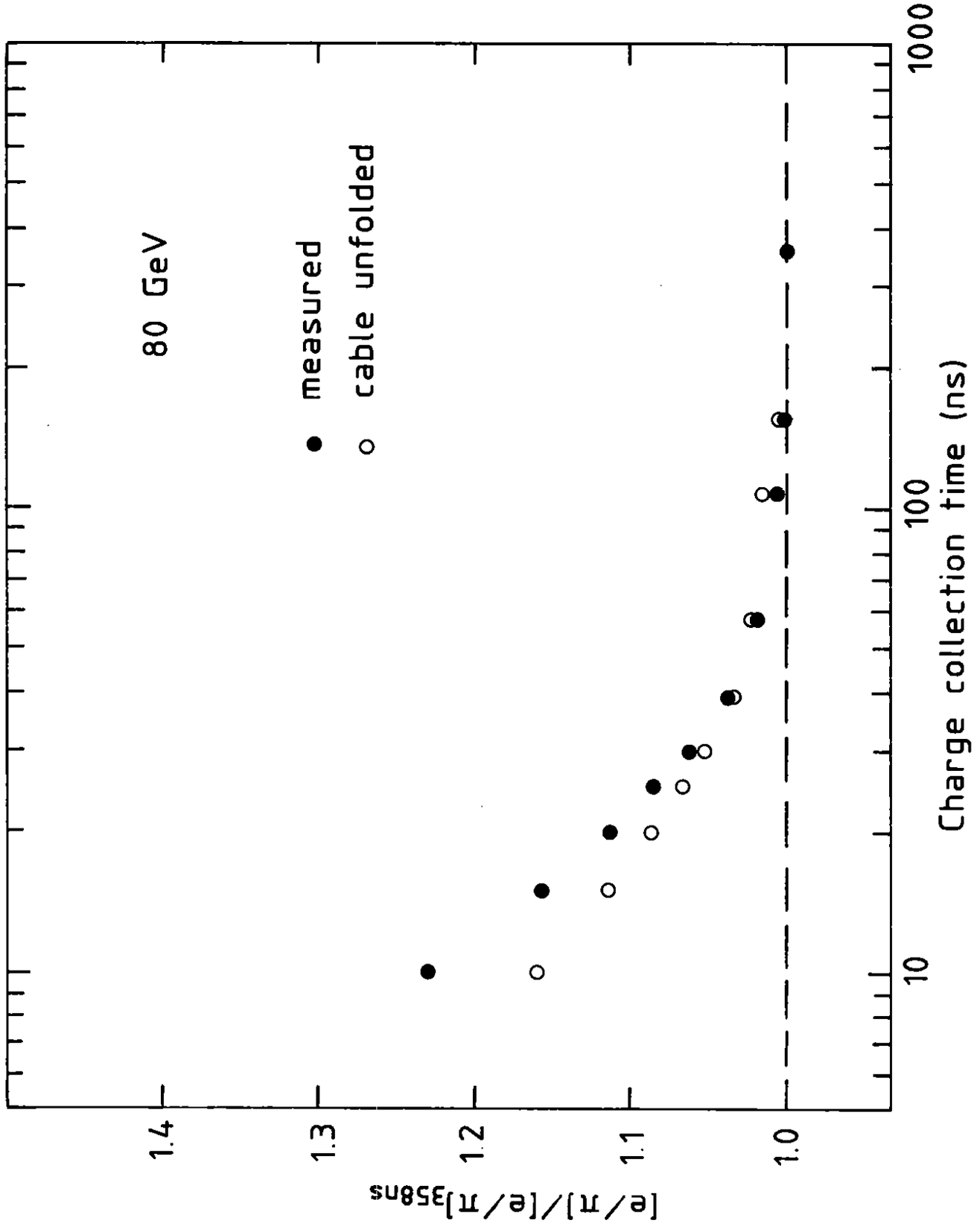
80 GeV
measured
cable unfolded
Charge collection time (ns)
10
100
1000
1.0
1.1
1.2
1.3
1.4
[e/π]/[e/π]35ns

Figure 13

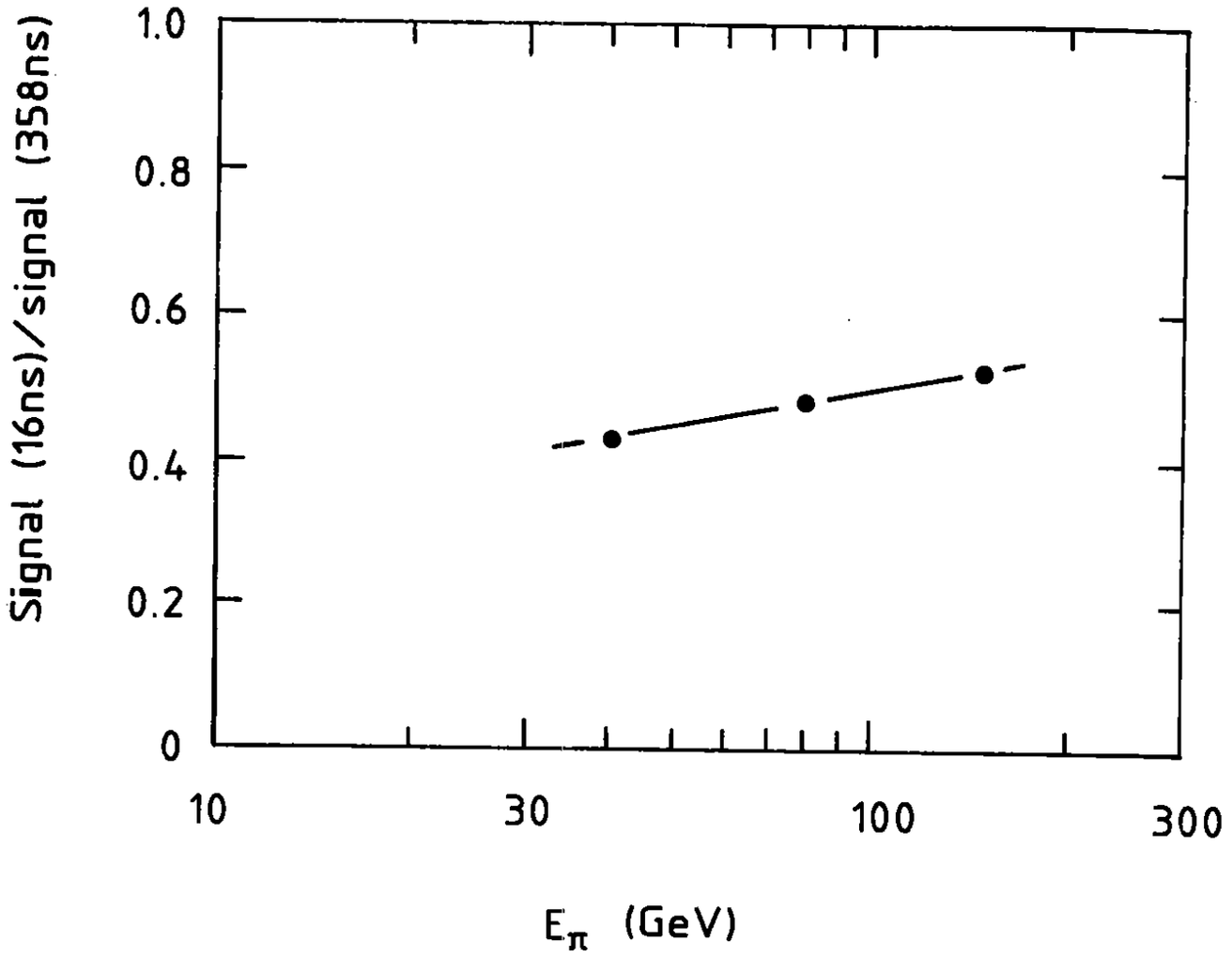

Figure 14

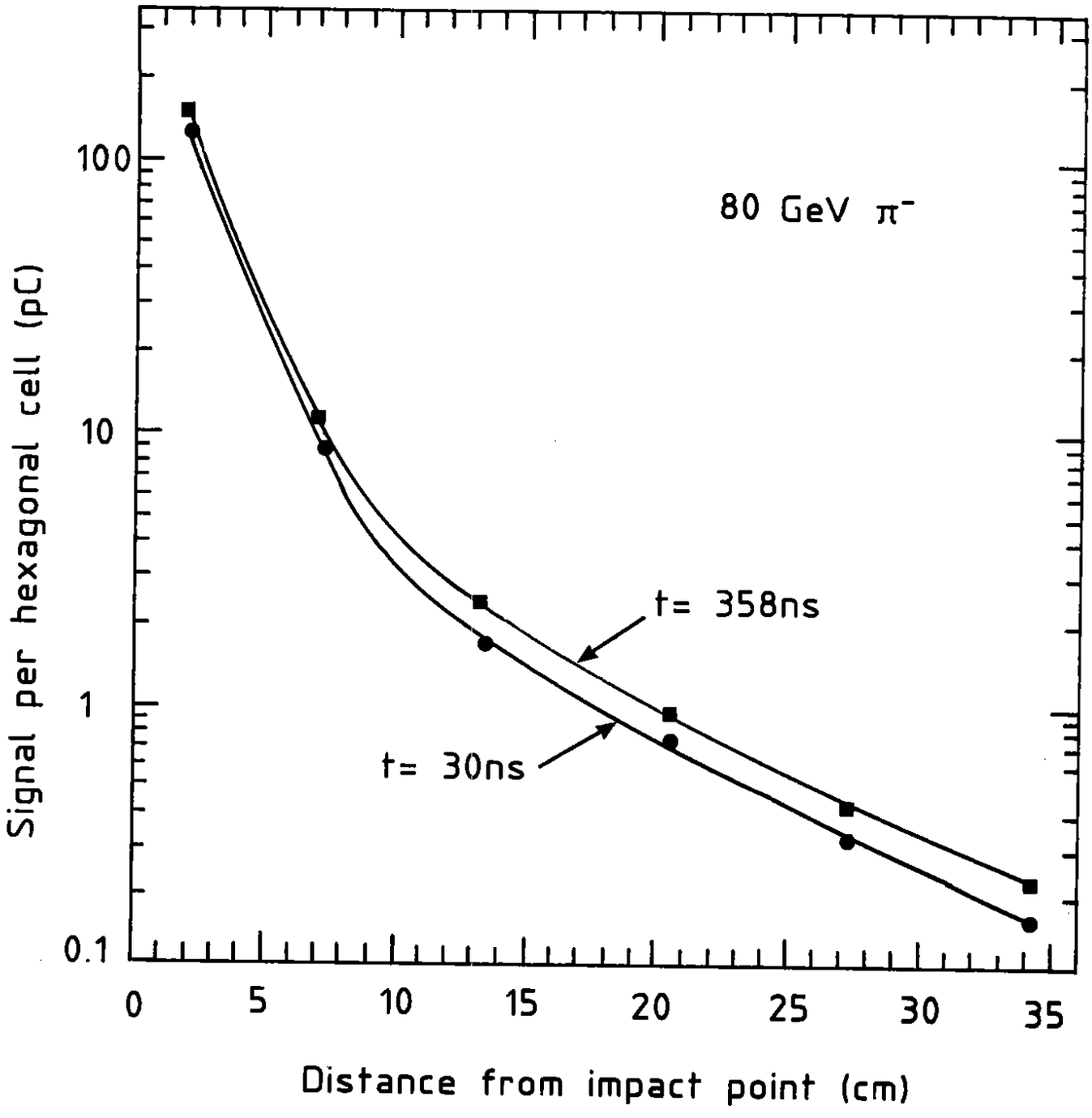
80 GeV π⁻
t= 358ns
t= 30ns
Signal per hexagonal cell (pC)
100
10
1
0.1
0
5
10
15
20
25
30
35
Distance from impact point (cm)

Figure 15

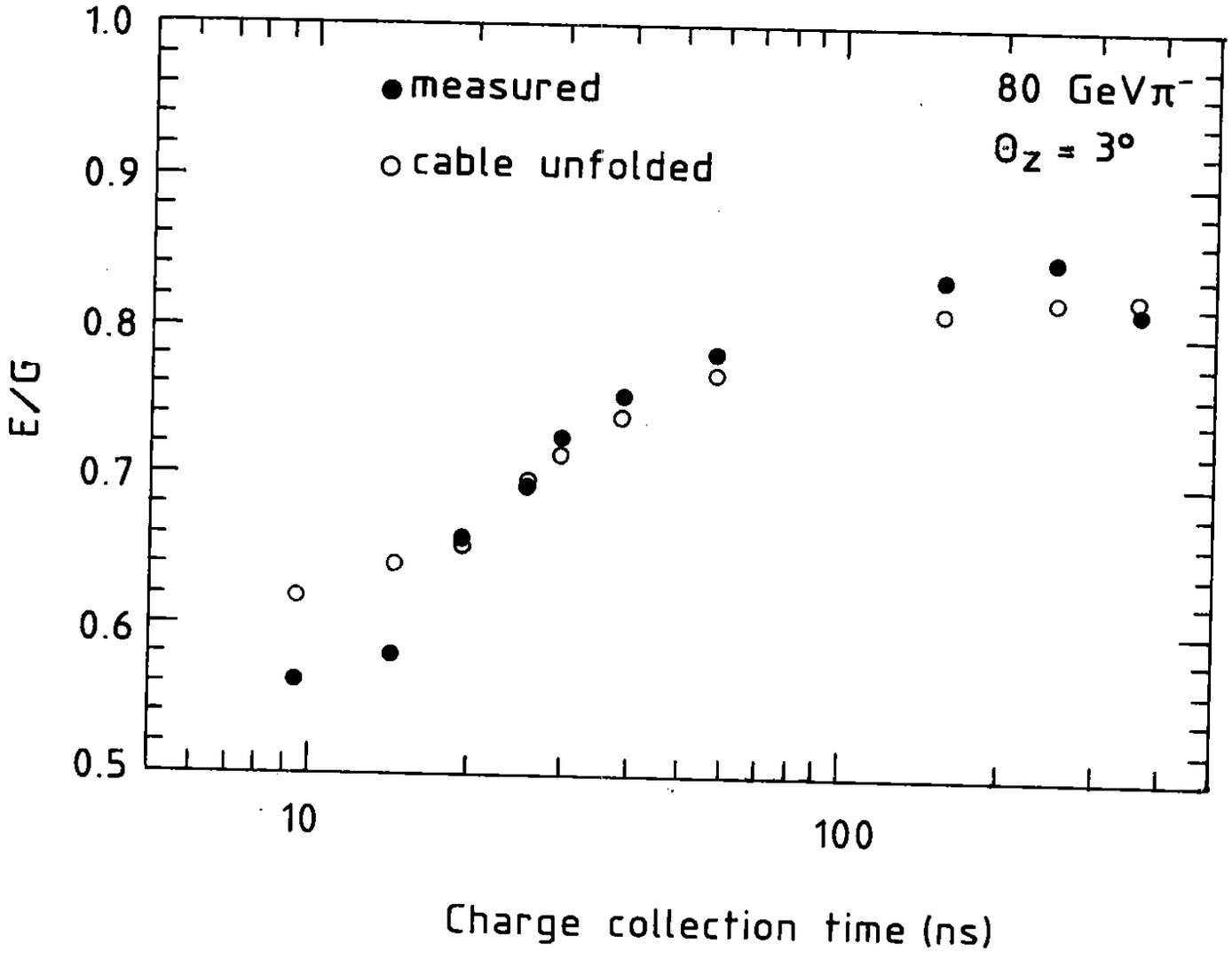
1.0
0.9
0.8
0.7
0.6
0.5
E/G
measured
cable unfolded
80 GeVπ⁻
θz = 3°
10
100
Charge collection time (ns)

Figure 16

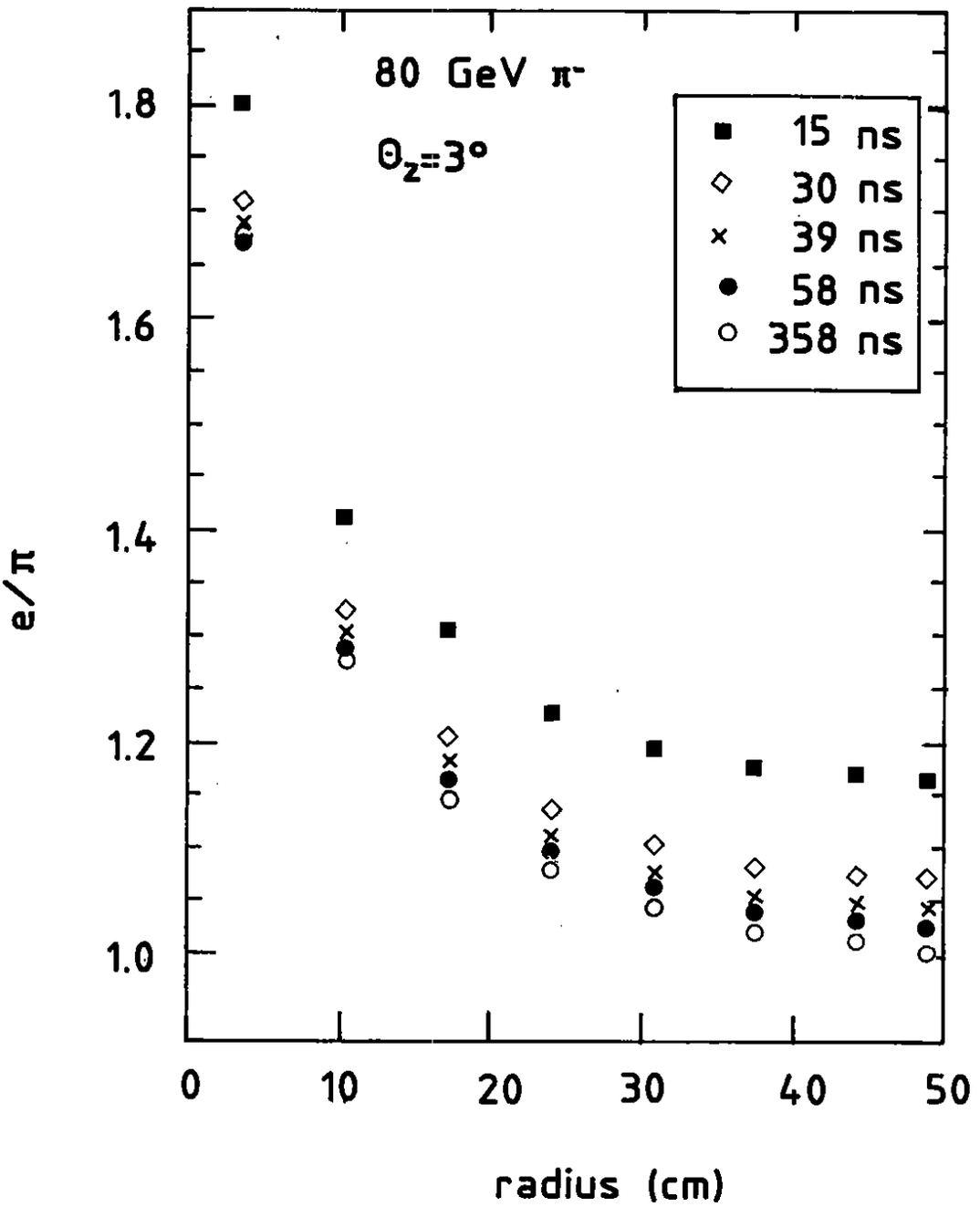
80 GeV π⁻
θz=3°
15 ns
30 ns
39 ns
58 ns
358 ns
e/π
1.8
1.6
1.4
1.2
1.0
0
10
20
30
40
50
radius (cm)

Figure 17

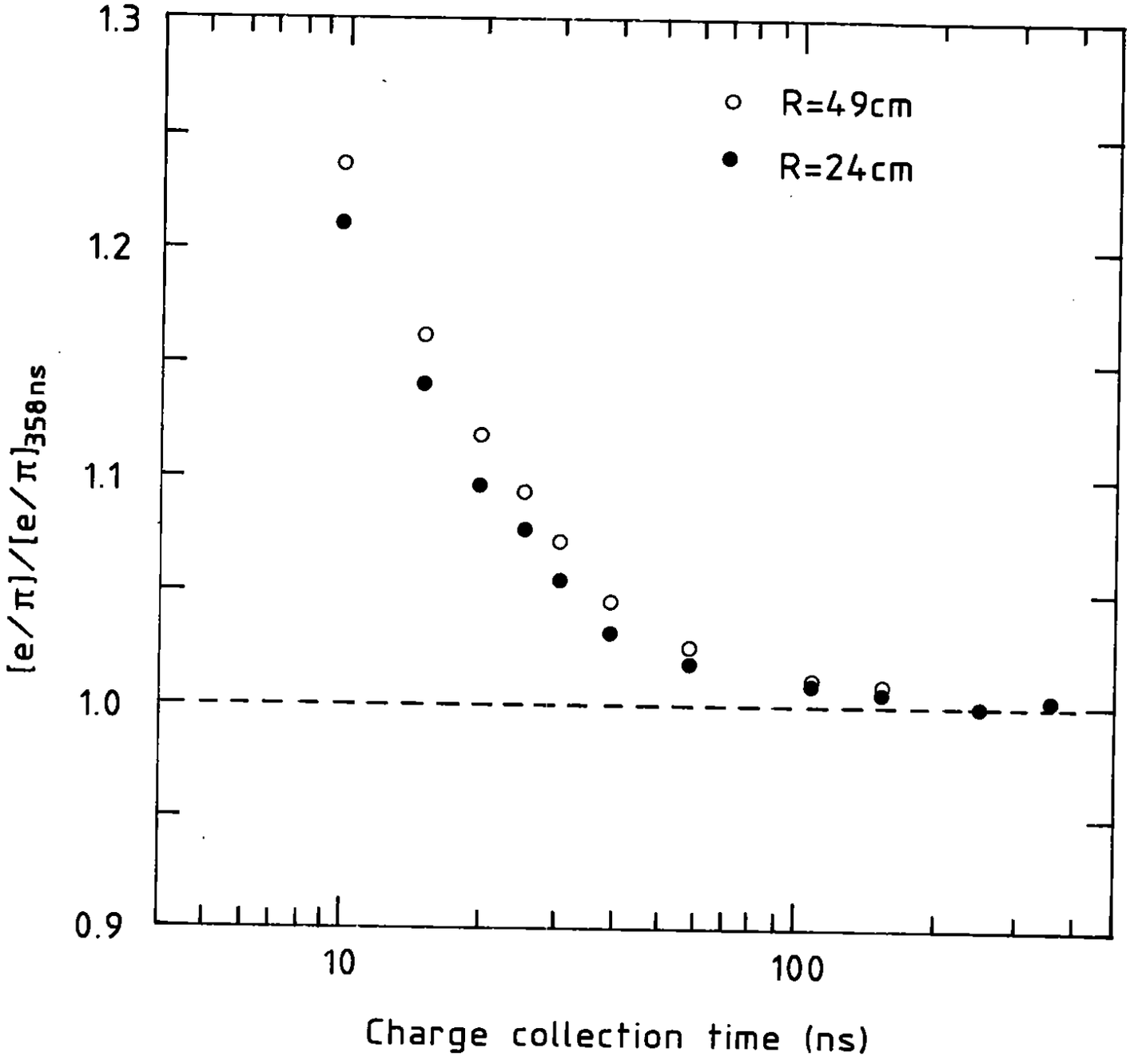
1.3
1.2
1.1
1.0
0.9
R=49cm
R=24cm
$[e/\pi]/[e/\pi]_{358ns}$
10
100
Charge collection time (ns)

Figure 18

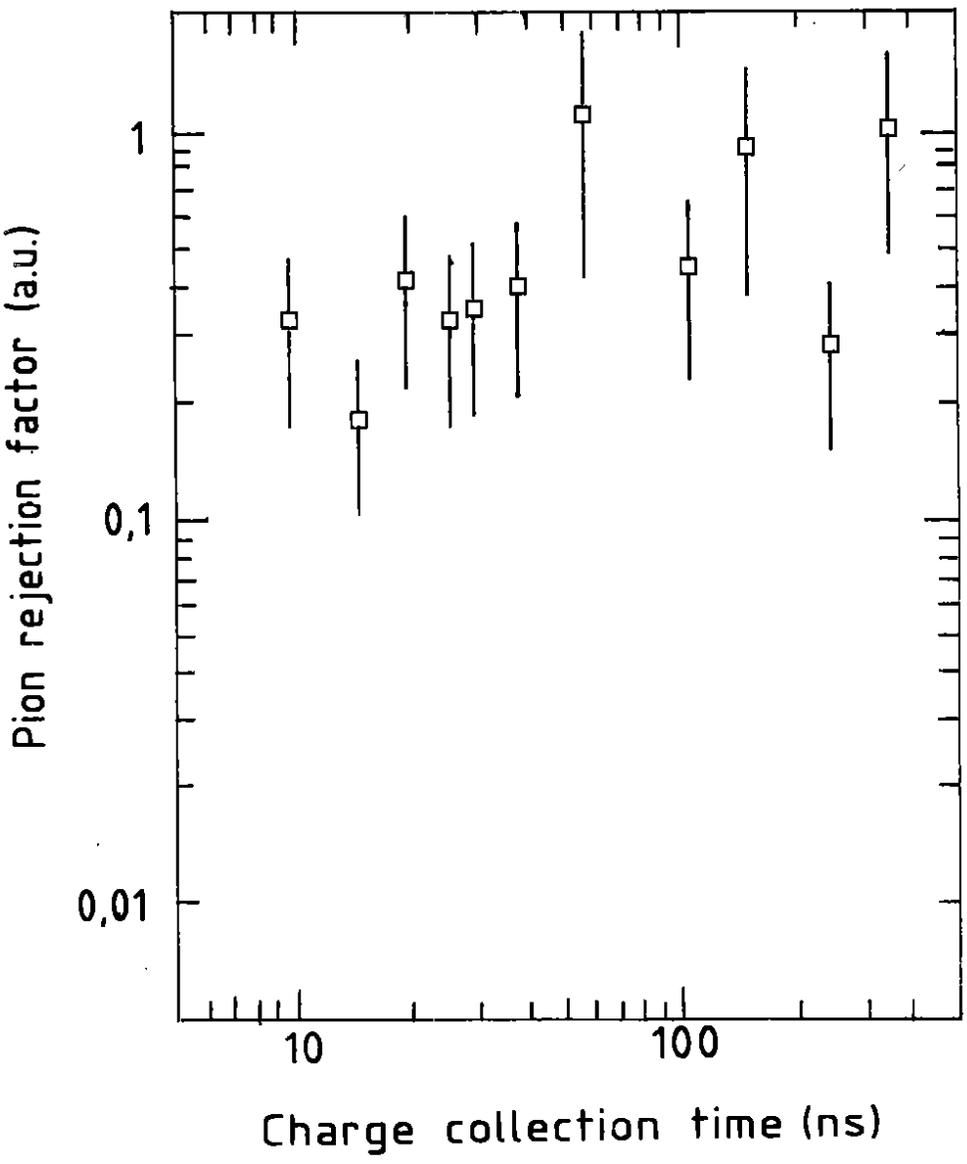
Pion rejection factor (a.u.)
1
0,1
0,01
10
100
Charge collection time (ns)

Figure 19

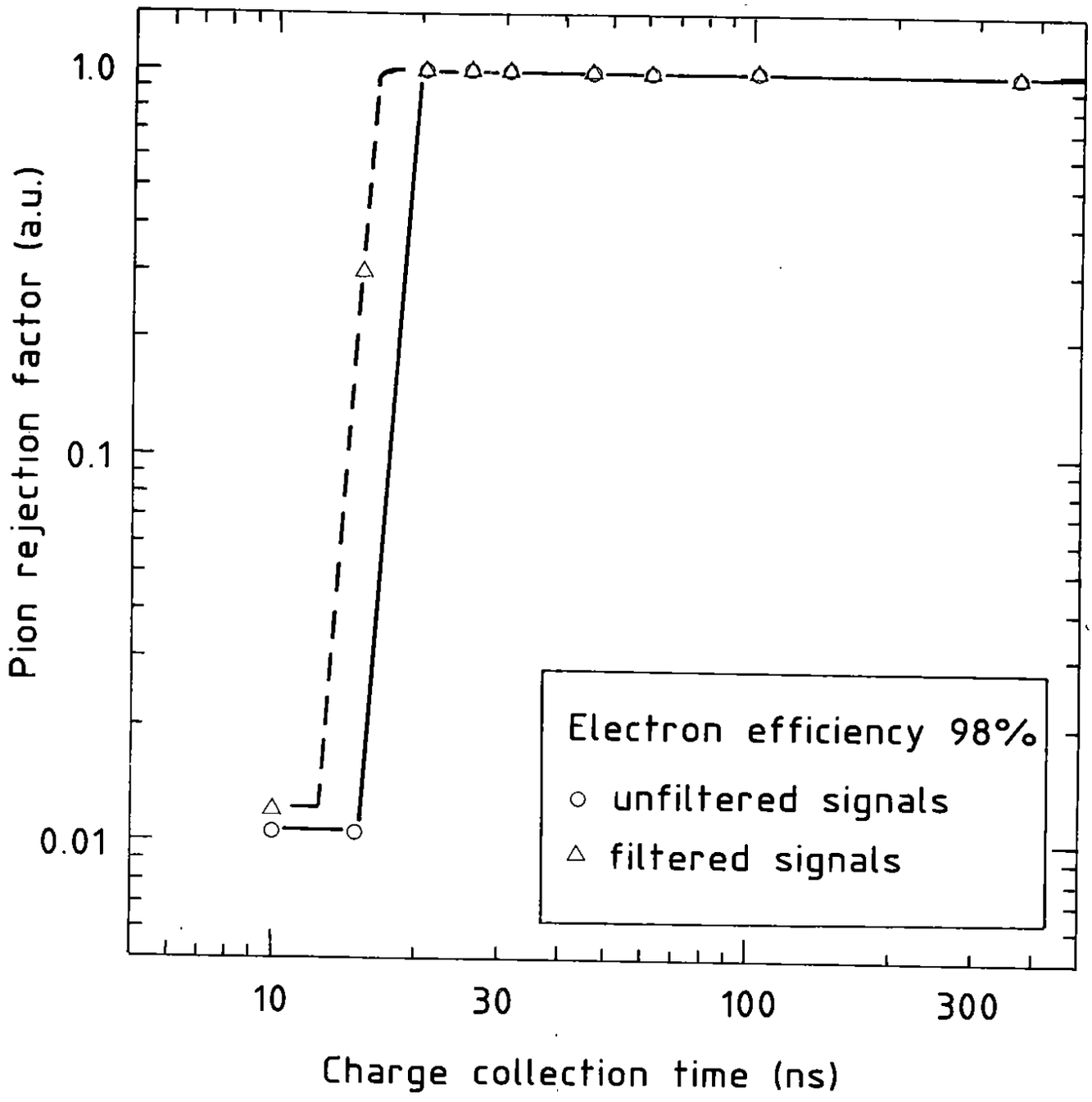

Figure 20

Imprimé au CERN. Prix : 1.50 Fr.